Approved for public release; distribution is unlimited.

The APL-UW Multiport Acoustic Projector System

by Rex K. Andrew

Technical Report
APL-UW TR 0902
December 2009

Applied Physics Laboratory University of Washington
1013 NE 40th Street Seattle, Washington 98105-6698

N00014-03-1-0181, N00014-07-1-0743, and N00014-08-1-0843

ACKNOWLEDGMENTS

Thanks are extended to Dr. Jack Butler of ImageAcoustics, Inc., who contributed helpful discussions during the development of the first tuner; Mr. Jan Lindberg of the Naval Undersea Warfare Center Newport for the loan of the MP200/TR1446; and Dr. Jim Mercer of APL-UW who negotiated to borrow the MP200/TR1446for APL-UW. This development effort was funded under ONR Grants N00014-03-1-0181, N00014-07-1-0743, and N00014-08-1-0843.

ABSTRACT

The Applied Physics Laboratory of the University of Washington (APL-UW) acquired on loan an experimental device known as the multiport transducer. APL-UW developed, in turn, a complete transmitter system that integrates this transducer, capable of wideband operation (roughly 180–350 Hz) from near-surface depths to depths greater than 1000 m. The system's electrical components include an autotransformer tuner, a battery power module, and a fibre optic telemetry interface; mechanical components include a steel supporting structure and a pressure-compensated tuner housing; an additional acoustical component is a monitor hydrophone in a vibration isolation mount; and a signal component involves a lumped parameter SPICE circuit model approximation of the entire end-to-end system, an associated C++ application to predict the time-domain acoustic far field from a standard time-domain waveform input file, and a pre-equalization filter. The multiport system was a key element in a 2009 at-sea ocean acoustics experiment located in the Philippine Sea and provided many hours of high-quality pulsed transmissions to a nearby vertical line array of hydrophones.

Contents

List of Figures

List of Tables

EXECUTIVE SUMMARY

The Applied Physics Laboratory of the University of Washington (APL-UW) acquired on loan an experimental device known as the multiport transducer. This device is a double ported free-flooded tube resonator, with resonances at about 210 Hz and 320 Hz. APL-UW developed, in turn, a complete transmitter system that integrates this transducer, which is described in this report.

The inventor of the multiport transducer (Dr. Jack Butler, ImageAcoustics, Inc.) maintains a finite-element model of the transducer, but for the purposes of the effort described here, a simpler lumped parameter equivalent circuit was developed that models the transfer of input voltage to "output" fluid velocity at the openings of the tubes. The system parameters were determined based on electrical and acoustical characteristics measured during an engineering test conducted by APL-UW in Lake Washington in 2006.

Transducers are usually mated to matching tuners, and several tuners were considered. In addition to tuning out the impedance mismatch at various frequencies, the tuners also served to step up the voltage into the transducer. This reduces the necessary voltage rating on the drive cable.

All the signal conditioning components from the digital-to-analog converter to the transducer were implemented as subcircuits in a SPICE model (Simulation Program with Integrated Circuit Emphasis; [1]), and incorporated into a C++ application code that takes an input file containing a time-domain waveform (encoded into 12-bit digital-to-analog words) and computes the time-domain far field pressure waveform. Various uses of this code are demonstrated: the RMS scaling difference between broadside source level and an endfire monitor sensor level, the wide band beam pattern, and actual source level calculations.

The transfer function into far field broadside pressure is significantly not flat but double-peaked, so there is a need to equalize the drive signal to mitigate the phase and amplitude distortion produced by the transducer. A pre-equalization filter was developed, and simulations demonstrate the efficacy of pre-equalization (based on the SPICE model transfer function) on pulse-compressed m-sequences.

The multiport system was a key element in a 2009 at-sea ocean acoustics experiment in the Philippine Sea and provided many hours of high-quality pulsed transmissions to a nearby vertical line array of hydrophones. A listing of these transmissions is provided in Appendix C.

1 Introduction

In 2005 the Applied Physics Laboratory of the University of Washington (APL-UW) acquired on loan an experimental device known as the "multiport" transducer from the Naval Undersea Warfare Center Division Newport. This transducer was originally designed and constructed by ImageAcoustics, Inc. [Cohasset, MA] and Massa Products, Inc. [Hingham, MA] under a Small Business Innovative Research (SBIR) grant to ImageAcoustics, Inc. from the Naval Undersea Warfare Center Division Newport.

APL-UW was subsequently funded by Code 321OA of the Office of Naval Research (ONR) to develop a deep-water ship-suspended system based around the MP200/TR1446 for operations in the ONR-sponsored Philippine Sea experiments of 2009 and 2010. This report summarizes that development effort. Section 2 describes the development effort for a simple circuit model suitable for routine system performance calculations. Some of these results have been disseminated in previous notes; the calculations regarding the transformation ratio are new. Chapter 3 describes the efforts made to design and build a tuner for the transducer. Section 4 describes the entire multiport system as built and deployed by APL-UW. Section 5 describes an entire system model of the multiport system, including the top-side electronics and the electro-opto-mechanical suspension cable, and the propagator to predict the far field time-domain radiated acoustic pressure. This model was incorporated for ease of use into a simulator code that takes as input a time-domain "drive" waveform in convenient standard `.wav` file format. Section 6 discusses the implementation of two different equalizers, necessary to compensate for the considerably non-flat response of the transducer itself. Finally, section 7 provides a review of the system in use during an at-sea deployment on an acoustics experiment in the Philippine Sea in 2009.

2 The Multiport Transducer

2.1 Introduction

The MP200/TR1446 is an experimental acoustic transducer invented and designed by Image-Acoustics, Inc. [Cohasset, MA] and built by Massa Products, Inc. [Hingham, MA; Fig. 1]. The theory of operation is fully described in the original patent [2]. In brief, it is a double ported free-flooded tube resonator, with resonances at about 210 Hz and 320 Hz. This device does not require pressurization, and can be driven to radiate at least 195 dB (narrowband) at any depth.

ImageAcoustics, Inc., maintains a complete model for this transducer, including a finite-element component to model the acoustic field inside the tubes. For the purposes of the development of the APL-UW system, it was not necessary to utilize their complete model. A simpler approximate model was developed at APL-UW and is presented in this section.

Figure 1: The MP200/TR1446. The orientation shown has the axis of the two tubes horizontal. From Refs. [3], [4].

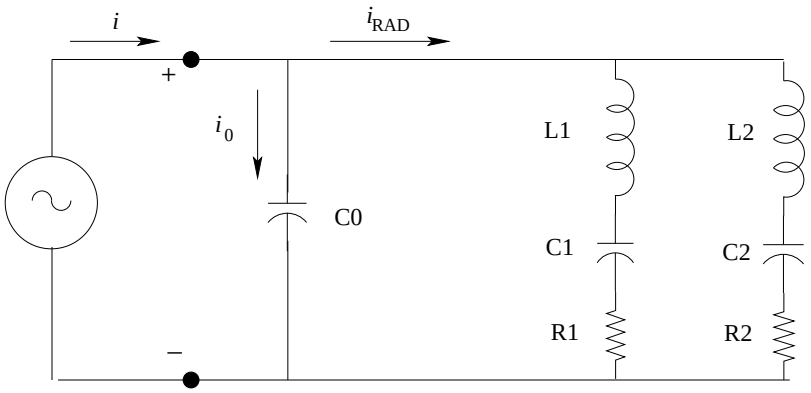

Figure 2: Simple equivalent electrical circuit for the Multiport Source. The "currents" i, i_0 and i_{RAD} are defined in section 2.5.

2.2 Equivalent Electrical Circuit — Theory

Characterization of the equivalent electrical circuit parameters follows the procedures of Wilson [5], Stansfield [6], and Sherman and Butler [7]. Given a power amplifier drive voltage of $v(t)$ with Fourier transform $V(f)$ and a drive current $i(t)$ with Fourier transform $I(f)$, the admittance is

$$Y(f) = \frac{I(f)}{V(f)} = G(f) + jB(f) \tag{1}$$

where $G(f)$ is the conductance and $B(f)$ is the susceptance, both in units of siemens, and $j = \sqrt{-1}$. The curves $G(f)$, $B(f)$ and the admittance locus $Y(f)$ can be used to determine various "raw" parameters, as described below, which are then converted to the elements of a simple equivalent circuit.

A simple but adequate equivalent circuit diagram (Fig. 2) represents the blocked capacitance of the device with a shunt capacitor, and the two tubes of the device with two parallel series RLC branches. There are two distinct resonances in the device, each represented by an RLC branch (Fig. 2), and these are far enough apart in frequency space that a separate analysis is pursued for each. The raw parameters and their computation are described below:

Low-Frequency Capacitance. The effective input admittance at low frequency goes as $B(\omega)/\omega$ as ω goes to zero and is represented by the capacitance C_{LF}.

Motional Resonance. The motional resonance frequency f_S is determined by locating the peak in the conductance $G(f)$.

Mechanical Q. The mechanical Q, denoted Q_M, is determined by the equation

$$Q_M = \frac{f_0}{f_2 - f_1} \tag{2}$$

where f_0 is a resonance frequency, and (f_1, f_2) are the frequencies where the conductance drops to half its maximum value at the resonance peak. These half-amplitude frequencies were calculated using linear (inverse) interpolation about $G = 0.5$.

Parallel Resonance. The parallel resonance frequency f_P is determined by finding the frequency $f_P > f_S$ where the $Y(f)$ locus meets the line from the origin to the point $(G(f_S), B(f_S))$ in the admittance plane.

Once these parameters have been determined, the following circuit parameters can be calculated:

Coupling Coefficient. The (squared) coupling coefficient is

$$k^2 = 1 - \frac{f_S^2}{f_P^2} \tag{3}$$

Mechanical Capacitance. The effective resonator mechanical capacitance, denoted by C, is roughly

$$C = k^2 C_{LF} \tag{4}$$

Resonance Inductance. The effective resonator mechanical inductance L is then related to C via the resonance frequency:

$$L = \frac{1}{\omega_S^2 C} \tag{5}$$

Blocked Capacitance. The blocked admittance is assumed here to be purely capacitative, and the capacitance is

$$C_0 = C_{LF} - C \tag{6}$$

Resonance Resistance. The resistance at resonance R is given roughly by

$$R = \frac{1}{\omega_S C Q_M} \tag{7}$$

2.3 2006 Lake Washington Test Configuration

APL-UW tested the MP200/TR1446 over the side of the R/V *Henderson* for several days in April 2006 in Lake Washington. The transducer was driven by an 80486 computer running MS-DOS and the program `atocsam`. The drive signal from the computer was routed to a Ling power amplifier and via the suspension cable to the transducer. A custom circuit internal to the Ling monitors the "top-of-the-cable" drive voltage and current.

An ITC 6050C hydrophone was deployed over the side of the R/V *Henderson* to monitor any acoustic emissions from the transducer. The hydrophone signal was routed into the "Tennelec" amplifier box (approximately no gain) through a Krohn–Hite filter (dialed to pass 100 Hz to 400 Hz at 0 dB), through an HP 4436A attenuator (set to 0 dB attenuation), and then into the "bare" signal input on the card cage chassis.

The input signal was generated via the application `seqsam` and consisted of an m-sequence with octal law 2033. The modulation angle was 88.2092°, 2 cycles per digit, 1023 digits. The carrier frequency was 250 Hz. As is customary with ATOC (acoustic thermometry of ocean climate) signals, the waveform was oversampled by a factor of 32, so the sampling rate of the playback digital–analog board was 8 kHz.

The program `atocsam` also performs simultaneous analog-to-digital while streaming out through the digital-to-analog (D/A) converter subsystem. In normal operation, five channels are captured: the 1 pulse/second line, power amplifier drive voltage monitor, power amplifier drive current monitor, "bare" acoustic input, and IRIG-M. Due to the high sampling rate, it was not possible to capture all five channels, and perform D/A, with the computer power available. Therefore, only three channels were captured: the voltage monitor, the current monitor, and the bare acoustic line.

Each test measurement was 120 s in duration. The programmable anti-alias filters on the filter/gain card were set to 384 Hz automatically by `atocsam`.

2.4 Equivalent Circuit Characterization — Results

With the Ling power amplifier, the voltage monitor circuit divides the power amplifier drive voltage by a factor of 1000, and the current monitor circuit converts the power amplifier drive current to a voltage by 200 mV/A.

In practice, $V(f)$ and $I(f)$ are computed using discrete Fourier transforms. In regions outside the main band of the signal, these terms are largely noise, and therefore only the admittance over the main frequency band $f \in [f_{\text{min}}, f_{\text{max}}]$ need be considered.

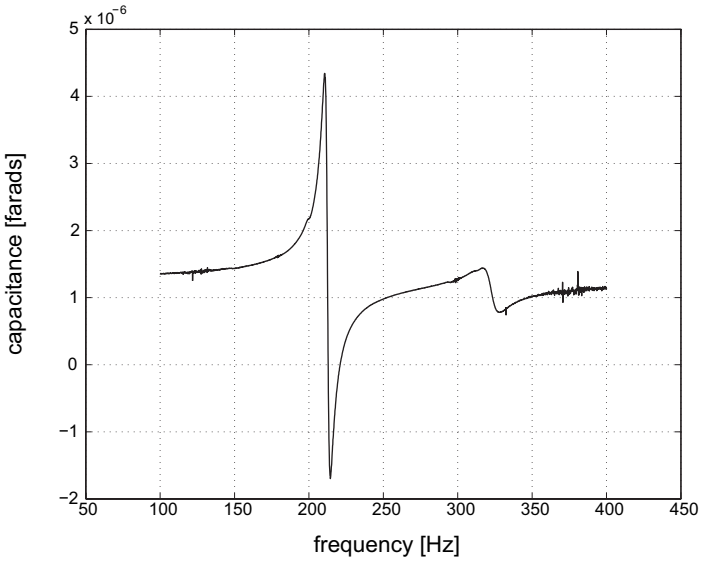

Figure 3: $B(\omega)/\omega$ versus frequency, 2006 Lake Washington test. File `mptest01.dat`.

In a 120-s transmission, there are 14 whole waveforms. Therefore, to mitigate additive system noise and increase the reliability of the admittance estimates, the 14 m-sequence waveforms were coherently averaged prior to the discrete Fourier transform step.

Low Frequency Capacitance. The effective input admittance at low frequency goes as $B(\omega)/\omega$ as ω goes to zero and is represented by the capacitance C_{LF}. In practice, the admittance loci were only calculated down to 100 Hz (because signal to noise issues progressively contaminated the result at lower frequencies). Furthermore, to moderate the effect of noise, the lowest five values of $B(\omega)/\omega$ were averaged. As an example, see Fig. 3.

Motional Resonance. The motional resonance frequency f_S is determined by locating the peak in the conductance $G(f)$. (The function was represented by a tab listing sampled at 122 mHz: here the frequency of the nearest frequency grid point was used.)

Mechanical Q. The mechanical Q is determined by Eq. 2, reproduced for convenience below:

$$Q_M = \frac{f_0}{f_2 - f_1}$$

where f_0 is a resonance frequency, and (f_1, f_2) are the frequencies where the conductance drops to half its maximum value at the resonance peak. These half-amplitude frequencies were calculated using linear (inverse) interpolation about $G = 0.5$.

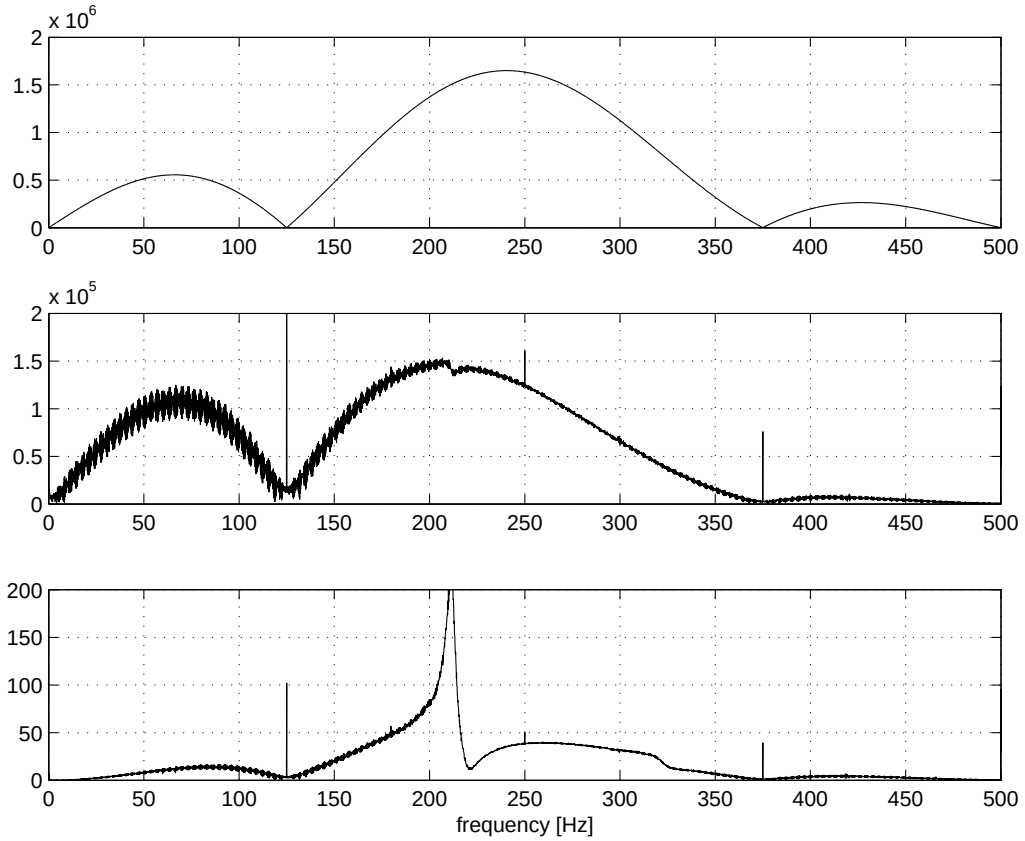

Figure 4: Fourier transforms of drive signals, 2006 Lake Washington test. Top: drive signal from file `mp001.sam`. Middle: power amplifier drive voltage from file `mptest15.sam`. Bottom: P.A. drive current from file `mptest15.sam`. The middle and bottom panels utilize the first m-sequence in the file.

The Fourier transforms of the drive signal and the voltage and current monitor channels for one m-sequence are shown in Fig. 4. The MP200/TR1446 has two resonances at approximately 200 and 300 Hz. Note that there is a smoothing filter after the D/A prior to the Ling to prevent high-frequency energy from entering the amplifier, and this can be seen in Fig. 4 causing an attenuation of the upper half of the main lobe and the upper sidelobe in the drive voltage transform. (This should have no effect on the admittance calculation because it causes an identical attenuation in both the drive voltage and current, and therefore cancels in their ratio.)

The computation of these parameters from an input admittance file was automated in a Matlab function, and applied to all the admittance files from the in-water 2006 Lake Washington test (with the exception of files corresponding to unusable transmissions.) Twenty-one transmissions were conducted. A summary of each collection is provided in

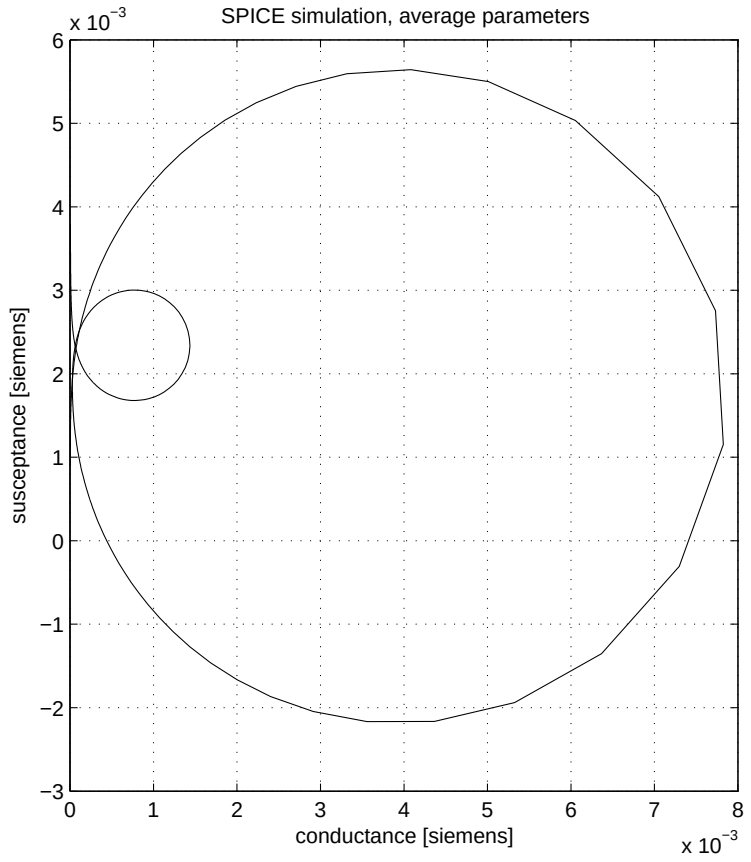

Figure 5: Admittance locus, SPICE simulation.

Appendix A. Summaries of the measured raw and computed values themselves are shown in Tables 1 and 2.

The admittance locus produced by a SPICE simulation is shown in Fig. 5. It bears good resemblance to the measured admittance loci (see Fig. 65 in Appendix A, for example).

2.5 Electro-Acoustic Transformation Ratio

To model the transducer from input voltage to output radiated acoustic field, a further refinement to the equivalent circuit model is needed. The standard approach is to utilize two transformation elements, one to transform between the electrical and mechanical stages, and the second to transform between the mechanical and acoustic stages. The approach taken here is much simpler: a single transformer is used to convert from the electrical stage to the acoustic field. This simplification is motivated by the lack (in this model) of internal

file	C_{LF}	f_{S1}	f_{P1}	Q_{M1}	f_{S1}	f_{P2}	Q_{M2}	comment
mptest01.dat	1.36E-006	212.61	221.29	56.66	322.22	326.13	28.30	150 ft
mptest02.dat	1.36E-006	212.61	221.41	57.16	322.59	325.88	28.41	150 ft
mptest03.dat	1.36E-006	212.61	221.53	57.72	322.46	326.01	28.87	150 ft
mptest04.dat	1.36E-006	212.61	221.66	57.76	322.22	326.25	28.92	150 ft
mptest05.dat	1.36E-006	212.61	221.78	57.89	322.59	326.13	28.88	150 ft
mptest06.dat	1.36E-006	212.61	221.90	57.85	322.71	326.13	28.88	150 ft
mptest07.dat	1.36E-006	211.88	220.92	53.90	321.36	324.17	26.79	shallow
mptest08.dat	1.36E-006	212.37	220.92	55.32	321.36	324.91	27.77	shallow
mptest11.dat	1.36E-006	212.37	221.66	57.33	321.97	325.40	28.27	shallow
mptest12.dat	1.35E-006	211.64	220.56	50.51	321.36	324.79	22.01	100 ft
mptest13.dat	1.36E-006	211.76	220.68	51.21	321.36	324.17	22.98	100 ft
mptest14.dat	1.35E-006	211.88	220.80	51.68	321.36	324.05	23.96	100 ft
mptest15.dat	1.35E-006	211.88	220.92	52.06	321.36	324.17	24.52	100 ft
mptest16.dat	1.35E-006	212.00	220.92	52.41	321.36	324.42	24.22	100 ft
averages:	1.36E-006	212.25	221.21	54.96	321.88	325.19	26.63	

Table 1: Raw parameters computed from admittance curves, 2006 Lake Washington test. All units are SI: farads and Hz. The Q is dimensionless.

file	C_0	C_1	L_1	R_1	C_2	L_2	R_2	comment
mptest01.dat	1.25E-006	1.04E-007	5.37	126.70	3.23E-008	7.55	539.77	150 ft
mptest02.dat	1.25E-006	1.06E-007	5.30	123.85	2.73E-008	8.90	634.97	150 ft
mptest03.dat	1.25E-006	1.07E-007	5.23	121.11	2.93E-008	8.30	582.66	150 ft
mptest04.dat	1.25E-006	1.08E-007	5.17	119.52	3.33E-008	7.32	512.50	150 ft
mptest05.dat	1.25E-006	1.10E-007	5.11	117.85	2.93E-008	8.31	583.04	150 ft
mptest06.dat	1.25E-006	1.11E-007	5.04	116.33	2.83E-008	8.59	602.79	150 ft
mptest07.dat	1.25E-006	1.09E-007	5.18	127.97	2.34E-008	10.46	788.33	shallow
mptest08.dat	1.26E-006	1.03E-007	5.44	131.28	2.95E-008	8.32	604.89	shallow
mptest11.dat	1.24E-006	1.11E-007	5.05	117.54	2.84E-008	8.62	616.62	shallow
mptest12.dat	1.25E-006	1.07E-007	5.27	138.82	2.84E-008	8.65	793.15	100ft
mptest13.dat	1.25E-006	1.07E-007	5.26	136.75	2.34E-008	10.48	921.15	100 ft
mptest14.dat	1.25E-006	1.07E-007	5.26	135.50	2.24E-008	10.96	923.24	100 ft
mptest15.dat	1.25E-006	1.09E-007	5.19	132.81	2.34E-008	10.49	863.61	100 ft
mptest16.dat	1.25E-006	1.07E-007	5.26	133.77	2.54E-008	9.67	805.89	100 ft
averages:	1.25E-006	1.08E-007	5.22	127.13	2.74E-008	9.04	698.04	

Table 2: Corresponding equivalent circuit parameter values, 2006 Lake Washington test. All units are SI: farads, henries, ohms.

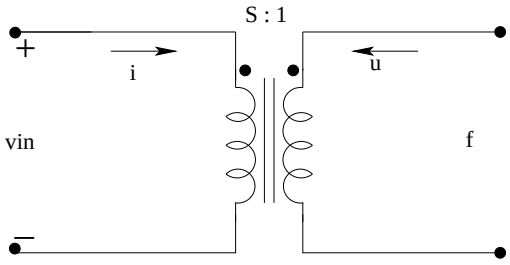

Figure 6: Electro-acoustic transformation element for the impedance analogy, converting from voltage and current in the electrical stage to force and velocity in the acoustic stage.

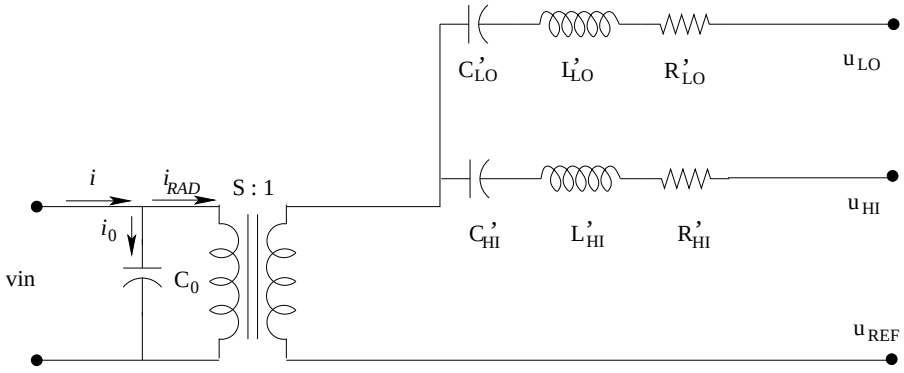

Figure 7: The modified equivalent circuit involving the transformation element.

mechanical and acoustic variables, and the need to only match input voltage levels to measured output acoustic levels. This "electro-acoustic transformer" is shown in Fig. 6. The modeling goal will be to determine the transformation ratio S, sometimes called the turns ratio.

First consider the lumped impedance analogy circuit (Fig. 7), which now includes the electro-acoustic transformer. At the resonance frequency of one of the branches, the velocity u in the transformer secondary will be dominated by the velocity "flowing" through that branch. The problem is separated into two distinct problems, one at each resonance frequency. Using the standard rules for transformers, the current and velocity are related according to

$$u = Si_{RAD} = \alpha Si \tag{8}$$

where α is the proportion of i that does not flow through the blocked capacitance C_0. This proportionality can be determined, e.g., from SPICE.

Next, consider the radiated acoustic field from one tube. The acoustic wavelength at resonance is much greater than the radius of the opening of that tube. The far field can be approximated to first order as if it originated from a "simple source" monopole located at

that end of that tube. This is true for both tubes. Thus, let

$$p_M(\mathbf{r}) = \frac{\Pi_M e^{ikr}}{4\pi r} \tag{9}$$

be the radiated pressure due to a monopole, where $|\mathbf{r}| = r$ and $i = \sqrt{-1}$. The source strength Π_M is related to the fluid velocity of the monopole via [8]

$$\Pi_M = \rho c k U \tag{10}$$

where $k = \omega/c$ and U is the volume velocity of the source. For a simple source with radius a, the volume velocity is $4\pi a^2 u_r$, where u_r is the radial velocity. A simple spherical source is not conceptually accurate for the MP200/TR1446; a better model might use a piston, with volume velocity $U = \pi a^2 u_z$, where u_z is now the velocity of the fluid at the opening of the tube, assumed constant over the opening, normal to the opening. The fluid velocity u_r or u_z is provided by the SPICE model: the choice of simple source or piston volume velocity is merely a matter of a constant of proportionality, but the choice must be consistent with the propagator used to calculate the far field (section 4). To maintain fidelity with the physical model,

$$\Pi_M = \pi a^2 \rho c k u_z \tag{11}$$

The two ends of the tube form an 'acoustic doublet,' shown schematically in Fig. 8. The total acoustic field at the field point is the superposition of the contributions from both sources. For measurements in the equatorial plane of the tube (i.e., $\mathbf{r} = [x_H, 0, 0]$), the two contributions are in-phase. Thus, if $x_H \gg L$ (where L is the length of the tube), the measured acoustic pressure is

$$|p_H(x_H)|^2 \approx 4|p_M(x_H)|^2 \tag{12}$$

Hence, using Eqs. 9, 11, and 12,

$$|u_z|^2 = \frac{4x_H^2}{a^2(\rho c)^2(ka)^2}|p_H(x_H)|^2 \tag{13}$$

Equating Eqs. 8 and 13, the far field pressure can be written as

$$|p_H(x_H)|^2 = B^2|i|^2 \tag{14}$$

i.e., the pressure is proportional to the drive current. The constant of proportionality, denoted here by B, consists of several factors:

$$B^2 = \frac{a^2(\rho c)^2(ka)^2\alpha^2 S^2}{4x_H^2} \tag{15}$$

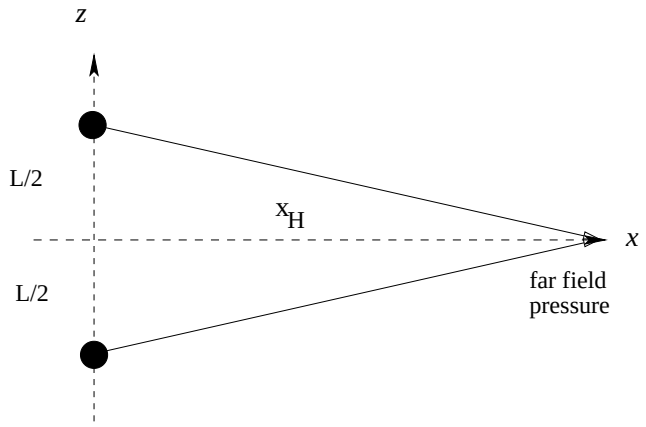

Figure 8: Acoustic doublet. A resonating tube or length L oriented vertically is represented by two in-phase equi-amplitude monopoles at $(0, 0, +L/2)$ and $(0, 0, -L/2)$. The field measurement is made at location $(x_H, 0, 0)$, where $x_H \gg L$.

If S were known from theory, B could be computed, and so too the far field pressure. This would be a prediction. The approach here is to utilize empirical measurements of the pressure and drive current to estimate S: Eq. 14 gives

$$\hat{B}^2 = \frac{|p_H(x_H)|^2}{|i|^2} \tag{16}$$

In principle, this is adequate to compute the pressure modulus at one location ($(x_H, 0, 0)$) and at one frequency. This ratio is likely to be frequency-dependent, and tabulating $\hat{B}(f)$ as a function of frequency is inconvenient. Rather, assuming that S is frequency-insensitive, we therefore seek to determine it explicitly. Thus,

$$S^2 = \frac{4x_H^2}{a^2\alpha^2(\rho c)^2(ka)^2}\frac{|p_H(x_H)|^2}{|i|^2} \tag{17}$$

To proceed further, it is required to estimate the drive current divider proportionality factor α, the range x_H, ka, the pressure magnitude at the field point $|p(x_H)|^2$, and the corresponding drive current magnitude $|i|$.

2.5.1 The Parameter ka

The dimensionless parameter ka, where a is the radius of either tube, is shown in Table 3 for both tubes. The full radius of the outer tube is used for the corresponding a for simplicity, although the radiating region is annular, and not πa^2. ka is less than unity in both cases.

tube length	diameter [m]	resonance [Hz]	ka
long	0.26	212	0.31
short	0.39	320	0.59

Table 3: Values of ka for both tubes.

file	peak bin	delay [ms]	range [m]
`mptest04.dat`	172	21.5	30.7
`mptest05.dat`	173	21.6	30.9
`mptest06.dat`	172	21.5	30.7

Table 4: Slant ranges from transducer to monitor hydrophone, 2006 Lake Washington test. Based on cross-correlation peak. Peak time converted to range using a typical freshwater sound speed of 1430 m/s.

2.5.2 Current Divider Factor

Using the simple circuit (Fig. 2), the proportionality factor $\alpha = |i_{RAD}|/|i|$ can be computed using SPICE. For the resonance frequencies 212 and 320 Hz, α is 0.98 and 0.54, respectively.

2.5.3 Field Point Range

The m-sequence used to interrogate the transducer is a useful ranging signal. By simply cross-correlating the drive voltage signal against the monitor hydrophone signal, the direct path arrival can be observed as the first prominent peak. For a sample rate of 8000 Hz, the sample period was 0.125 ms. Three transmissions from the 2006 Lake Washington exercise were found to have acceptable drive current and monitor channel data. Table 4 shows the ranges estimated for these three transmissions.

2.5.4 Field Pressure

The monitor channel data autospectra were estimated for each corresponding file using the Matlab command

```
[G,f] = pwelch(x,kaiser(8192),0,8192,8000,'onesided');
```

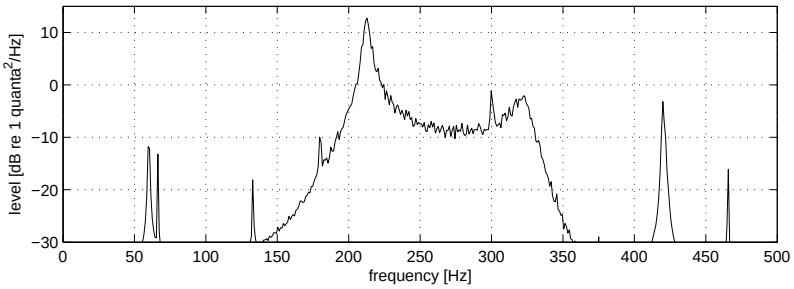

Figure 9: An estimated monitor hydrophone autospectrum, 2006 Lake Washington test, file `mptest06.dat`.

This routine provides an autospectral estimate in units of quanta^2/Hz. An example autospectrum is shown in Fig. 9.

The ITC 6050C hydrophone had a terminal sensitivity of -178.2 dB V/μPa, and the A/D converter was set to convert 5V into 2048 quanta, or 52.2 dB quanta/V. The total channel had a transfer function of -126.0 dB quanta/μPa, and was essentially frequency independent in the circuit passband. The levels of the resonance peaks were extracted and converted to in-water face-of-phone units (Table 5).

	pressure		current	
file	$G_{qq}(212)$	$G_{pp}(212)$	$G_{qq}(212)$	$G_{ii}(212)$
`mptest04.dat`	12.8	138.7	20.1	-24.2
`mptest05.dat`	12.9	138.9	20.2	-24.1
`mptest06.dat`	12.6	138.6	20.3	-24.0
average		138.7		-24.1
amplitude		8.64 $\times 10^6 \mu$Pa		6.24×10^{-2} A
file	$G_{qq}(320)$	$G_{pp}(320)$	$G_{qq}(320)$	$G_{ii}(320)$
`mptest04.dat`	-2.1	123.9	0.2	-44.0
`mptest05.dat`	-2.0	124.0	0.3	-44.0
`mptest06.dat`	-2.0	124.0	0.3	-44.0
average		123.4		-44.0
amplitude		1.58 $\times 10^6 \mu$Pa		6.3×10^{-3} A

Table 5: Radiated pressure and drive current magnitudes for the three transmissions, resonances of 212 Hz and 320 Hz, Lake Washington 2006 test. The averages were computed in decibel space. Units are dB re 1 quanta^2/Hz for $G_{qq}(f)$, dB re 1 μPa^2/Hz for $G_{pp}(f)$, and dB re 1 A^2/Hz for $G_{ii}(f)$.

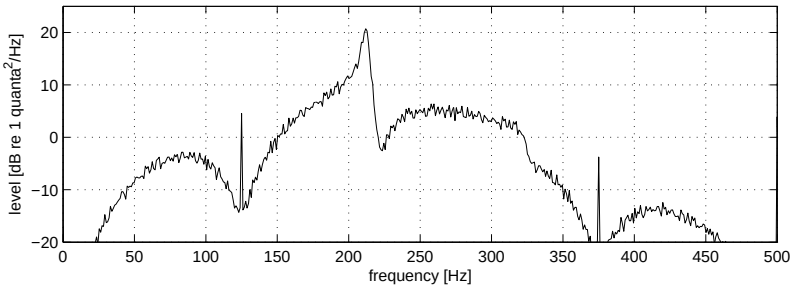

Figure 10: An estimated drive current autospectrum, 2006 Lake Washington test, file `mptest06.dat`.

resonance [Hz]	S^2	S
212	5.70×10^9	7.55×10^4
320	7.56×10^9	8.69×10^4
"average"		8.12×10^4

Table 6: Transformation ratios calculated from the 2006 Lake Washington data. Density was 1000 kg/m^3, and sound speed was 1430 m/s. All other values given in the text.

2.5.5 Drive Current

The drive current data autospectra were similarly estimated for each corresponding file using the Matlab command

```
[G,f] = pwelch(x,kaiser(8192),0,8192,8000,'onesided');
```

This routine provides an autospectral estimate in correct units of quanta^2/Hz. An example autospectrum is shown in Fig. 10.

The current monitoring circuit had a calibration of 0.0061 quanta/A. The levels of the autospectra at the resonance frequencies are also provided in Table 5.

2.5.6 Incorporating the Transformation Ratio

Using the values of field pressure level, slant range, drive current level, the local sound speed, and coarse estimates of density and simple source radii, values for the transformation ratio can be calculated at resonance frequencies of 212 and 320 Hz (Table 6).

Using the electro-acoustic transformer, it is now possible to "reflect" the two resonant branches from the electrical equivalent circuit to the acoustic stage. The "average" trans-

element	initial value	transformed value
C_{LO}	1.08×10^{-7}	712
L_{LO}	5.22	7.92×10^{-10}
R_{LO}	127	1.93×10^{-8}
C_{HI}	2.74×10^{-8}	181
L_{HI}	9.04	1.37×10^{-9}
R_{HI}	698	1.06×10^{-7}

Table 7: Lumped acoustical equivalent circuit values for the resonant branch components.

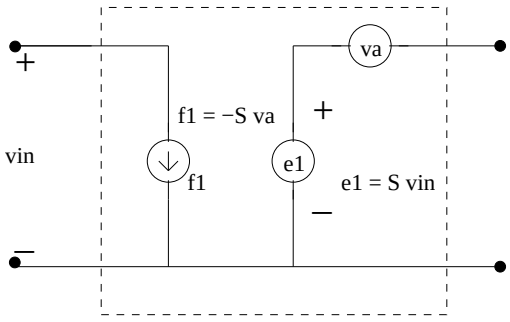

Figure 11: SPICE representation of an ideal transformer with transformation ratio S.

formation ratio was used in this calculation. This reflection is not necessary, but it makes clear the separate functionality of the acoustic components. The resulting equivalent circuit is shown in Fig. 7 and the transformed circuit quantities in Table 7.

SPICE provides a transformer element, but it is too realistic to use here. The proper "ideal transformer" is shown in Fig. 11. The "secondary" consists of a voltage source $e1$ equal to S times the primary voltage, and a "voltage sensor" va. The voltage sensor supplies no additional voltage, but is a mechanism for measuring the current out of the secondary. The "primary" consists of a current source $f1$ that drives a current S times that flowing out of the secondary. The formal SPICE circuit corresponding to the modified equivalent circuit Fig. 7 is shown in Fig. 12.

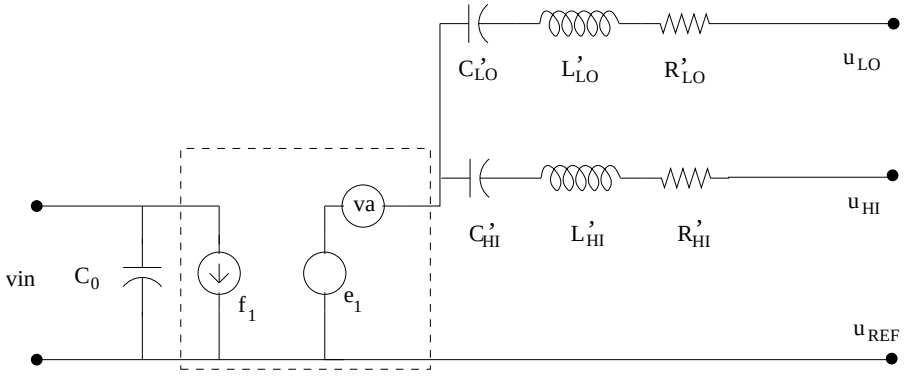

Figure 12: The SPICE circuit corresponding to the circuit of Fig. 7.

3 Tuning

It is advantageous to add a tuner/transformer to a high-power piezoceramic transducer for two reasons:

1. The inductance of the tuner/transformer can be used to match the capacitance of the piezoceramic itself, resulting in a better power factor at the power amplifier, which results in more efficient transfer of power to the transducer;

2. The voltage on the suspension cable can be kept within rated levels by utilizing a tuner/transformer at the underwater package that includes a step-up ratio.

An autotransformer is generally used in this application, because electrical isolation is not required, and the autotransformer does not require as massive a core as a conventional transformer.

3.1 Single Resonance Theory

Consider an example circuit (Fig. 13). At the resonance frequency, the untuned circuit has a power factor of 0.55; the admittance loop is shown in Fig. 14. An inductance value of 50 mH brings the power factor to 0.996: the resulting admittance loop is also shown in Fig. 14.

Using the equation

$$P(f) = \frac{1}{2}V(f)^* I(f) = W(f) + jQ(f) \tag{18}$$

for the average complex power, a SPICE calculation at the resonance frequency shows that the ratio of real power delivered by the source (W) to total power $|P(f)|$ goes from 55% to 100%, corresponding to the power factor. Delivery of power at this frequency is optimized by this inductor.

3.2 Multiple Resonance Theory and Wideband Signals

The conventional approach presented in the previous section is defined for a system with a single resonance at a single frequency. It is not obvious, however, how to extend those results to a system with multiple resonances and wideband signals.

Drs. Birdsall and Metzger (University of Michigan) compute power for the HX554 transducers fabricated under the ATOC program as follows. Given time-domain voltage $v(t)$ and current $i(t)$ at the driving point, the power is

$$W = \frac{1}{T}\int_0^T v(t)i(t)\,dt \tag{19}$$

Based on the Schwarz inequality, the quantity

$$\frac{|W|}{\sqrt{\frac{1}{T}\int |v(t)|^2\,dt\;\frac{1}{T}\int |i(t)|^2\,dt}} \tag{20}$$

will always be less than or equal to unity. The value of unity is obtained if $v(t)$ is linearly related to $i(t)$. Furthermore, for $v(t) = V_0\cos(\omega t)$ and $i(t) = I_0\cos(\omega t + \phi)$, this expression yields the single frequency power factor of $\cos\phi$. Eq. 20 is therefore a candidate "broadband power factor."

Consider a circuit (Fig. 15) involving two parallel branches to represent the two resonances of the transducer. It includes a tuning inductor L_p. Several values for this tuning inductor are used: 220 mH, 300 mH, and 450 mH (see section 3.3). The additional values provide coverage around the broadband power factor peak. The time domain drive signal was an m-sequence with 1023 bits, a Q of 2, and carrier frequencies of 250, 275, and 300 Hz. These options span the likely values envisioned for the multiport system. The drive current was computed by inverse Fourier transformation of the input admittance product (as computed by SPICE) and the drive signal transform (Table 8).

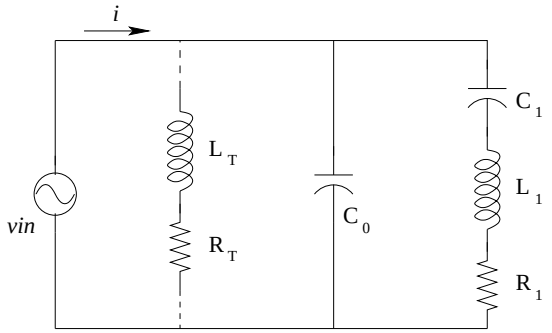

Figure 13: Tuning example circuit. The shunt inductor L_T is added to compensate for the reactance in the parallel combination of the C_0 capacitor and the series *R-L-C* branch. The resistor R_T is included to model the small resistance in the inductor windings. $C_0 = 10\mu$F, $C_1 = 0.1\mu$F, $R_1 = 100\,\Omega$, and $L_1 = 5$ H. The tuning inductor is $L_T = 50$ mH, and $R_T = 0.1\,\Omega$. The resonance frequency is ≈ 225 Hz.

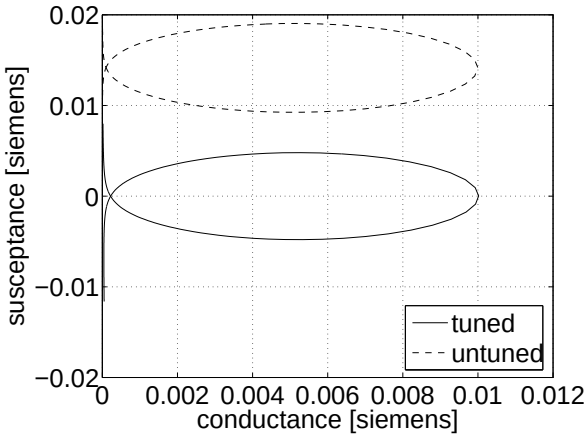

Figure 14: Admittance loops for the single resonance circuit, with and without the tuning inductor.

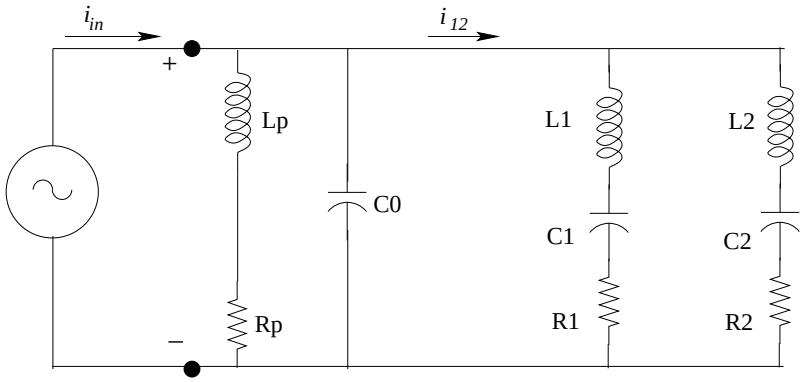

Figure 15: Simple electrical equivalent SPICE model of transducer with a parallel tuning inductor. A resistor R_p is included with the inductor to prevent a short circuit shunt path at DC in SPICE analysis. R_p is 1 Ω.

	carrier frequency		
L_p	250 Hz	275 Hz	300 Hz
220 mH	09.0%	08.7%	08.2%
300 mH	11.6%	11.1%	10.4%
450 mH	15.0%	14.0%	12.6%
600 mH	16.5%	15.1%	13.2%
850 mH	17.3%	15.4%	13.2%
1000 mH	17.3%	15.4%	13.1%
1250 mH	17.2%	15.1%	12.8%

Table 8: "Broadband power factor" for the circuit of Fig. 15 and an m-sequence drive signal.

Optimal tuning does not bring this measure near 100%, as was the case in the single frequency example. Indeed, over the values of tuning inductance used, there is little significant change in this measure. If the broadband power factor were interpreted as $\cos\phi$, then the phase angle is generally 85° to at best 80°. Furthermore, there is a slight dependence on the drive signal itself, a feature that complicates the design of the optimal tuning inductance. Alternatively, the measure is not strongly sensitive to these drive signals, so an approximate, albeit suboptimal, tuning inductance value could be determined using essentially any signal from a given class of target signal types.

This multiple resonance example, unlike the single one, shows that it is neither simple nor straightforward to optimally tune a system for a broadband signal, especially a system with multiple resonances. (On a similar note, John Watson of APL-UW [9] advised that a computer analysis be performed over the full band to gauge the efficacy of a tuner.)

The electrical power calculated by Eq. 19 is all real, i.e., "active" power, and does not include reactive power.

3.3 The 1:2 Tuner

Dr. Jack Butler and Victoria Curtis at ImageAcoustics, Inc., considered the equivalent circuit of Fig. 15 and suggested optimal values for the parallel inductor L_p based on the following argument. The curves of conductance and susceptance against frequency for the untuned circuit (i.e., without a parallel inductor) are shown in Fig. 16. Using a design goal of achieving the greatest number of zero-crossings (or zero-touchings) of the susceptance curve, they chose a parallel inductance value of 0.296 H. This moves the susceptance curve down until four points either touch or cross the axis: see Fig. 17.

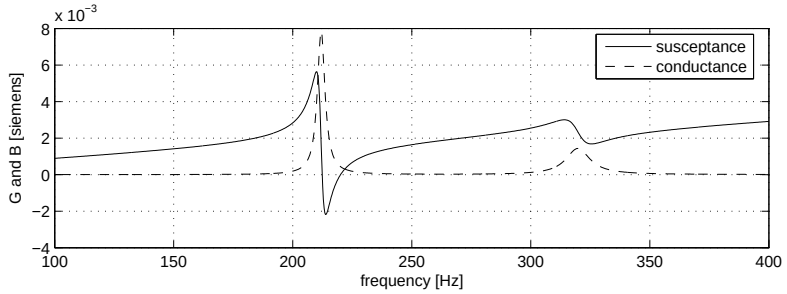

Figure 16: Conductance and susceptance of the circuit, no tuning inductor.

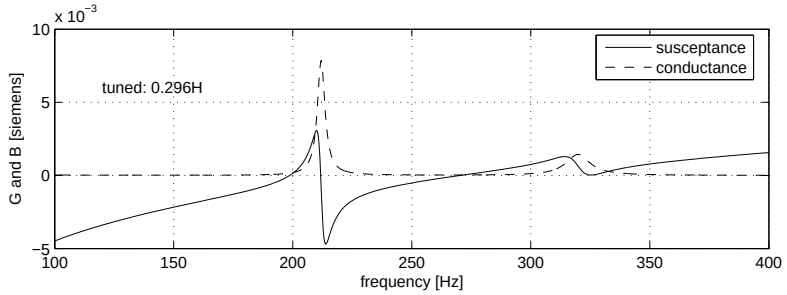

Figure 17: Conductance and susceptance of the circuit, tuning shunt inductor of 0.296H, shunt resistance of 1 ohm.

As alternatives, two other shunt inductances were considered, designed to cancel the susceptance at either of the two resonances, in accord with the simpler single-resonance problem.

The first autotransformer/tuner was therefore specified to have shunt inductances of 220 mH, 300 mH, and 450 mH. The device was also specified to have a step-up ratio of primary to secondary voltages of 1:2.

The contract for this device was awarded to Coiltron, Inc. [Tigard, OR]. Pictures of the device when delivered are shown in Figs. 18 and 19 . Concern regarding heat build-up in the device led APL-UW to provide two thermistors to Coiltron during the winding process to be inserted deep inside the windings, near the core, for monitoring during operation. Leads from these thermistors can be seen in the pictures.

The housing for the tuner was designed and fabricated at APL-UW (Figs. 20 and 21). The housing was filled with oil to act as a convective heat-transfer coolant during operation, and also to compensate hydrostatic pressure. Concern regarding thermal expansion of the oil when heated led to the addition of an oil exchange system (Fig. 22), which has tubing to connect oil in the housing with two expansion tanks.

Figure 18: Corner view of the first tuner.

Figure 19: End view of the first tuner.

Figure 20: Housing for the tuner.

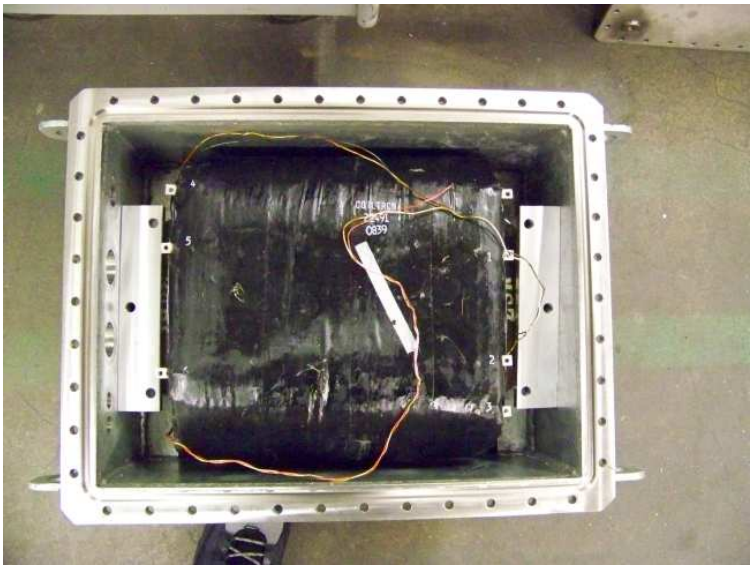

Figure 21: Top view looking inside the tuner housing, with tuner in place.

Figure 22: Tuner and housing completely assembled. Note the oil expansion system tubing and expansion tanks. Also visible on top (protected with a bracket) is an over-pressure relief valve.

3.4 The 1:3 Tuner

The 1:2 tuner did not provide enough output voltage (see section 7.3), so a 1:3 tuner was designed. In the SPICE circuit for this tuner (Fig. 23), the autotransformer is modeled as two magnetically coupled inductors, with values L_{p1} and L_{p2}, respectively. There is an additional resistance associated with each inductor for modeling the resistive loss through the windings. The magnetic coupling factor used in the calculations was 0.98.

The equations governing the autotransformer are as follows. The primary voltage v_1 and primary current i_1 are related to the secondary voltage v_2 and secondary current i_2 by

$$v_1 = j\omega L_{p1}(i_1 + i_2) + j\omega M i_2 \quad (21)$$

$$v_2 = j\omega L_{p2} i_2 + j\omega L_{p1}(i_1 + i_2) + j\omega M i_1 \quad (22)$$

where M is the mutual inductance, defined according to the magnetic coupling factor K as

$$K = \frac{M}{\sqrt{L_{p1} L_{p2}}}. \quad (23)$$

The simplest analysis assumes perfect coupling (i.e., $K = 1$, and therefore $M = \sqrt{L_{p1} L_{p2}}$) and an open circuit secondary. In this case, $i_2 = 0$ and the equations above become

$$v_1 = j\omega L_{p1} i_1 \quad (24)$$

$$v_2 = j\omega L_{p1} i_1 + j\omega \sqrt{L_{p1} L_{p2}}\, i_1 \quad (25)$$

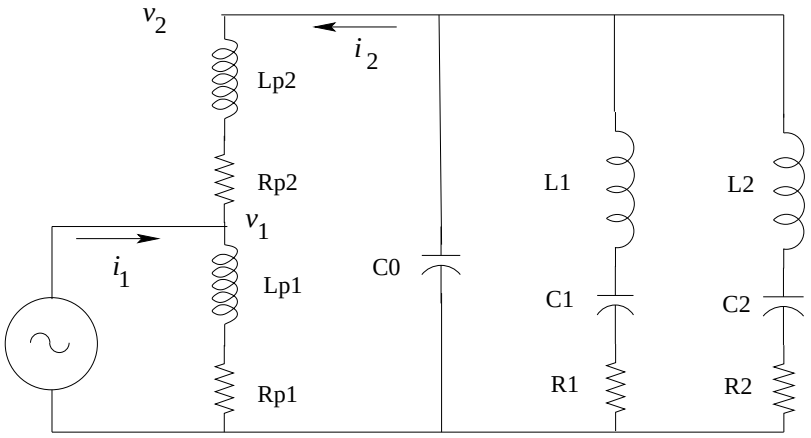

Figure 23: Simple electrical equivalent SPICE circuit involving the autotransformer.

Solving for the output/input ratio, one obtains

$$\frac{v_2}{v_1} = 1 + \sqrt{\frac{L_{p2}}{L_{p1}}} \tag{26}$$

This approximation is valid when the inductive reactance is much greater than the series resistance in each winding, and the secondary load is large compared to the inductive reactance seen across the entire secondary. This will in general not be the case when operating near the tuned frequency, but this approximation does provide a useful crude formula to verify the step-up ratio of the autotransformer.

(The choice of lower and upper inductance values — here L_{p1} and L_{p2} — to meet a required step-up ratio and overall inductance involves more complexity than is represented in Eq. 26 [pers. comm., Richard Gettmann, 13 July 2009]. Therefore, Eq. 26 should be interpreted as a rough guide for choosing the two inductance values. It remains true that Eq. 26 provides a good model for the output of the corresponding SPICE circuit.

The design goal was to achieve a step-up from the primary to the secondary of about a factor of 3, and to adjust the susceptance curve about zero. This was done by trial-and-error at each of the two resonance frequencies, thereby determining the "optimal" solution for each. The middle option was devised as was done for the 1:2 tuner, by determining those values that caused four crossings or touchings of the susceptance curve with the zero axis. The resulting parameter values are shown in Table 9.

The admittance loops for these three cases are shown in Figs. 24, 25, and 26, and it can be seen for the lower and upper resonances that the proper choice of autotransformer inductors centers the corresponding admittance loop on the zero axis. The "middle" tuning configuration centers neither on the zero axis.

	L_{p1}	L_{p2}
low freq	50 mH	210 mH
mid freq	33 mH	130 mH
hi freq	22 mH	90 mH

Table 9: Upper and lower inductor values for tuning the circuit, at three different frequencies, 1:3 step-up.

The corresponding conductance and susceptance curves for these three cases are shown in Figs. 27, 28, and 29. The "middle" tuning can be verified here as that configuration that causes four crossings or touchings.

As an additional verification, the tuner output (autotransformer secondary) is plotted versus frequency for all three tuning configurations in Figs. 30, 31, and 32. The input voltage in all cases was uniform across all frequencies at $1 + 0j$. These figures indicate that the autotransformer secondary output is load dependent for these load magnitudes, but that the output–input ratio is close to the design value of 3 for all frequencies considered.

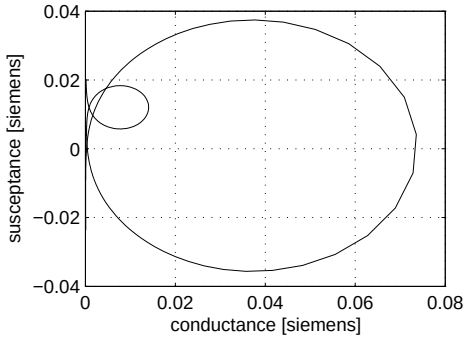

Figure 24: Admittance loop, tuned for the lower (212 Hz) resonance frequency.

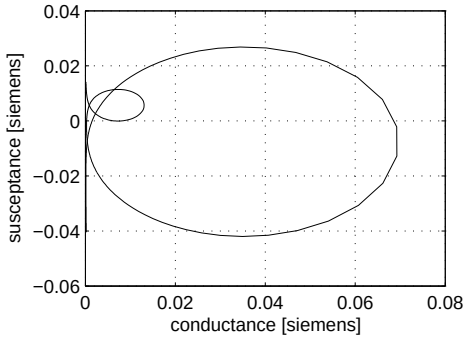

Figure 25: Admittance loop, tuned between the resonances.

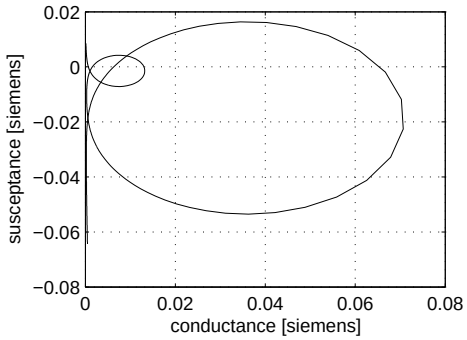

Figure 26: Admittance loop, tuned for the upper (320 Hz) resonance frequency.

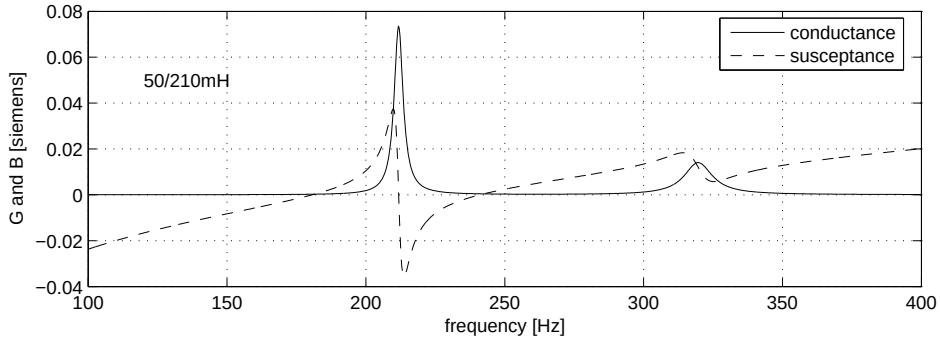

Figure 27: Conductance and susceptance curves, tuned for the lower (212 Hz) resonance frequency.

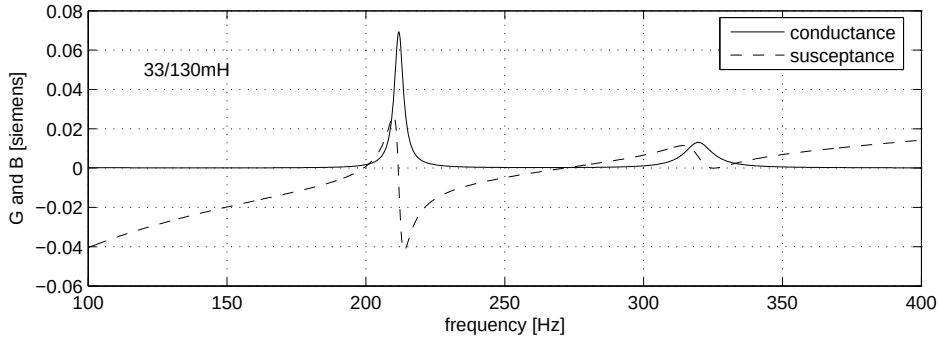

Figure 28: Conductance and susceptance curves, tuned between the resonances.

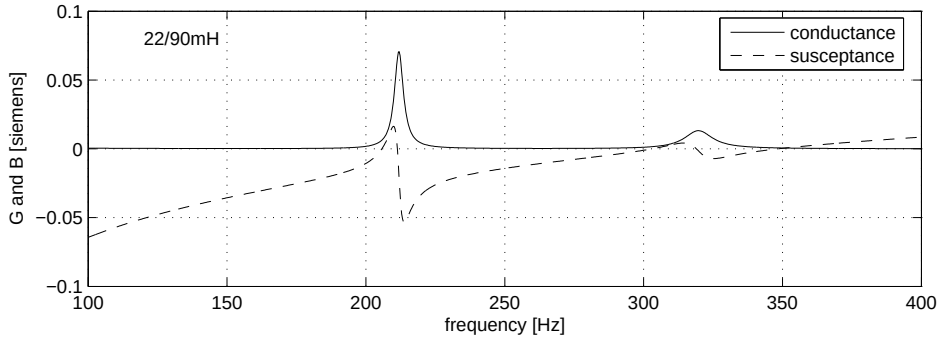

Figure 29: Conductance and susceptance curves, tuned for the upper (320 Hz) resonance frequency.

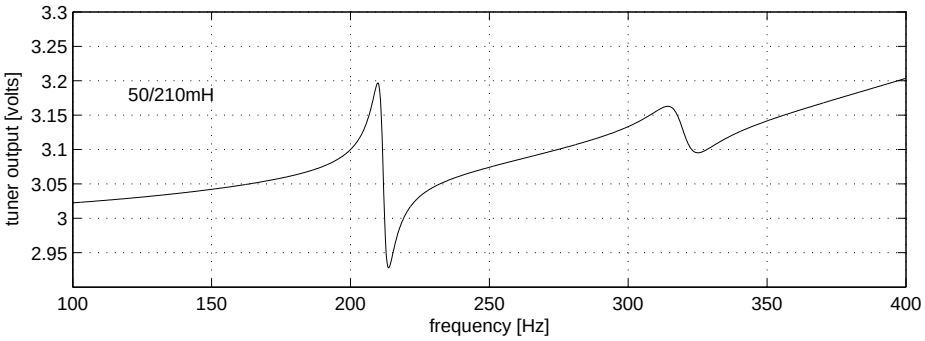

Figure 30: Tuner voltage across the secondary. The input voltage was unity. Circuit tuned for the lower (212 Hz) resonance frequency.

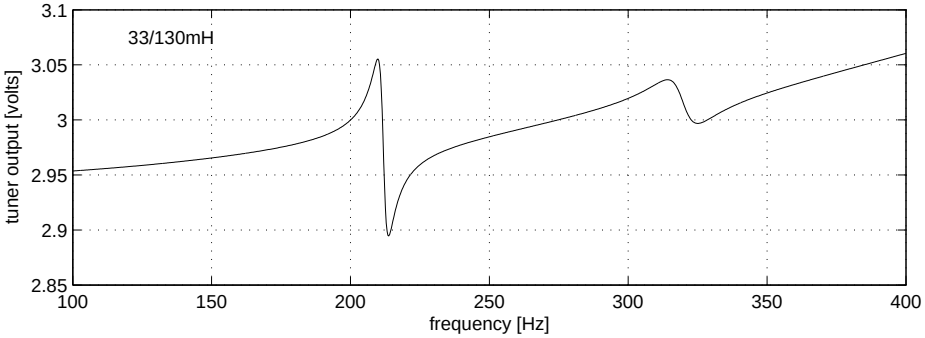

Figure 31: Voltage across the secondary. The input voltage was unity. Circuit tuned between the resonances.

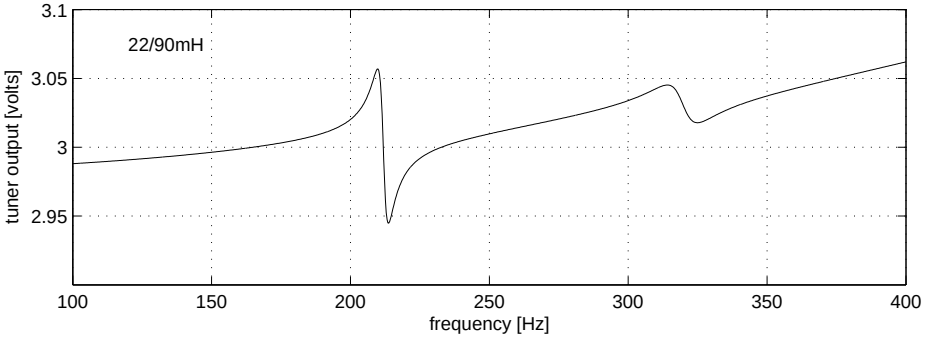

Figure 32: Voltage across the secondary. The input voltage was unity. Circuit tuned for the upper (320 Hz) resonance frequency.

4 The Multiport System

An essential system block diagram of the APL-UW system (Fig. 33) shows the underwater subsystem components:

- the MP200/TR1446 with the tuner
- a monitor hydrophone
- a custom telemetry bottle with a fibre-optic interface
- a depth sensor
- a SeaBattery

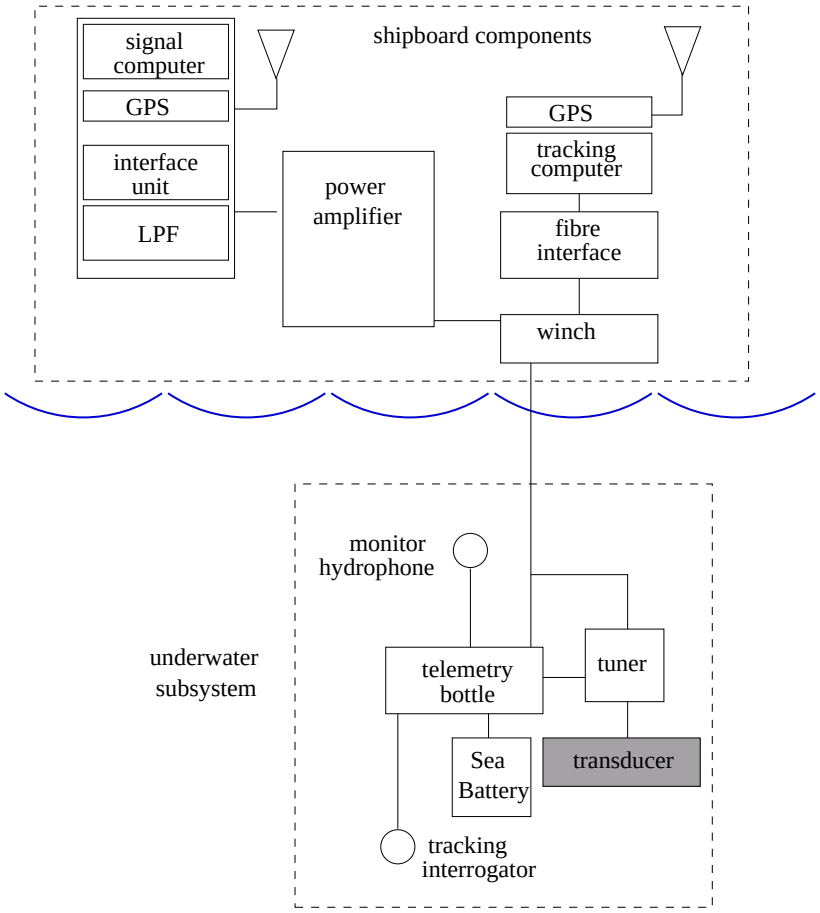

Figure 33: Block diagram of essential components for the complete multiport system.

The ship-side equipment consists of a signal delivery rack, which includes a 80686 PC running Fedora Core 8 Linux, a Spectrum Instruments TM-4 GPS receiver, a custom interface unit, and a Krohn–Hite filter; a power amplifier; a custom winch; and a tracking system. The original power amplifier was a Ling. An L50 amplifier was procured from Instruments, Inc., for the Philippine Sea experiments.

The underwater package is suspended from an "electro-opto-mechanical" cable. Telemetry information utilizes the fibre, and transducer power utilizes the copper conductor. In practice, the underwater package is deployed and recovered by the custom winch.

An ITC 6050C hydrophone will normally be deployed on the transducer axis at a known, fixed distance (typically 20 m) above the acoustic center of the main tube. The raw time-domain acoustic signal is digitized in the telemetry bottle, multiplexed onto the optical fibre, demultiplexed and reconstructed back to an analog signal within the shipboard fibre interface, and supplied to the signal computer for recording. Initial measurements of this channel (not including the hydrophone) indicate that the channel has a passband level of -5.5 dB between about 7 Hz and 5000 Hz.

Under the assumption that the acoustical performance of the MP200/TR1446 itself would be compromised if anything was attached to it, the mechanical configuration hung the auxiliary components (SeaBattery, telemetry bottle, and tuner) above the MP200/TR1446 (Fig. 34). In this design, the MP200/TR1446 itself would be stowed on-board deck horizontally.

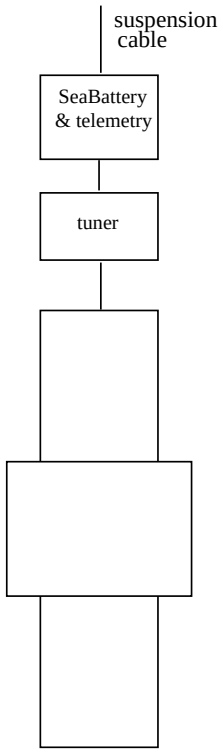

Figure 34: Schematic of the initial mechanical configuration.

Subsequently, in consultation with ImageAcoustics, it was determined that the configuration in Fig. 34 would mass-load the fluid in the main tube and alter the resonant and radiation properties of the device. (It was also realized that the chain of components may be extremely difficult to deploy.)

The mechanical design evolved so that the auxiliary components were relocated to the equator of the MP200/TR1446 and placed on opposite sides for balance (Fig. 35). An auxiliary structure was designed that both supported the auxiliary components and also

supported the MP200/TR1446 in an upright position while on deck. Although massive, the SeaBattery and the tuner were small relative to a wavelength, and therefore their modification to the radiated acoustical field should be small as long as they are away from the tube openings. The support structure itself was fabricated from free-flooded steel tubing, which also should have a negligible acoustical cross-section. No modeling has been done to quantify the effect of these auxiliary components on the radiated acoustical field.

With the design complete, it was realized that the entire system would be too tall to be lifted from the deck using a chain bridle attached to the bolt eyes fixed into the top of the main tube. A tentative plan was devised to lift from a hard point welded onto the main tube exactly at the top of the secondary tube, i.e., lifting the entire system from one "shoulder." This plan introduced a further problem: the system would hang at an angle significantly off vertical. Further calculations showed, however, that a lifting point located at the center of a cross-bar bolted into the mouth of the main tube several centimeters down from the top would provide enough clearance. The cross-bar width was much less than a wavelength and overall cross-sectional area much less than the area of the main tube opening, so this bar is not expected to modify the resonant or radiation patterns significantly. In the final analysis, the system was calculated to hang about 2.6° off vertical.

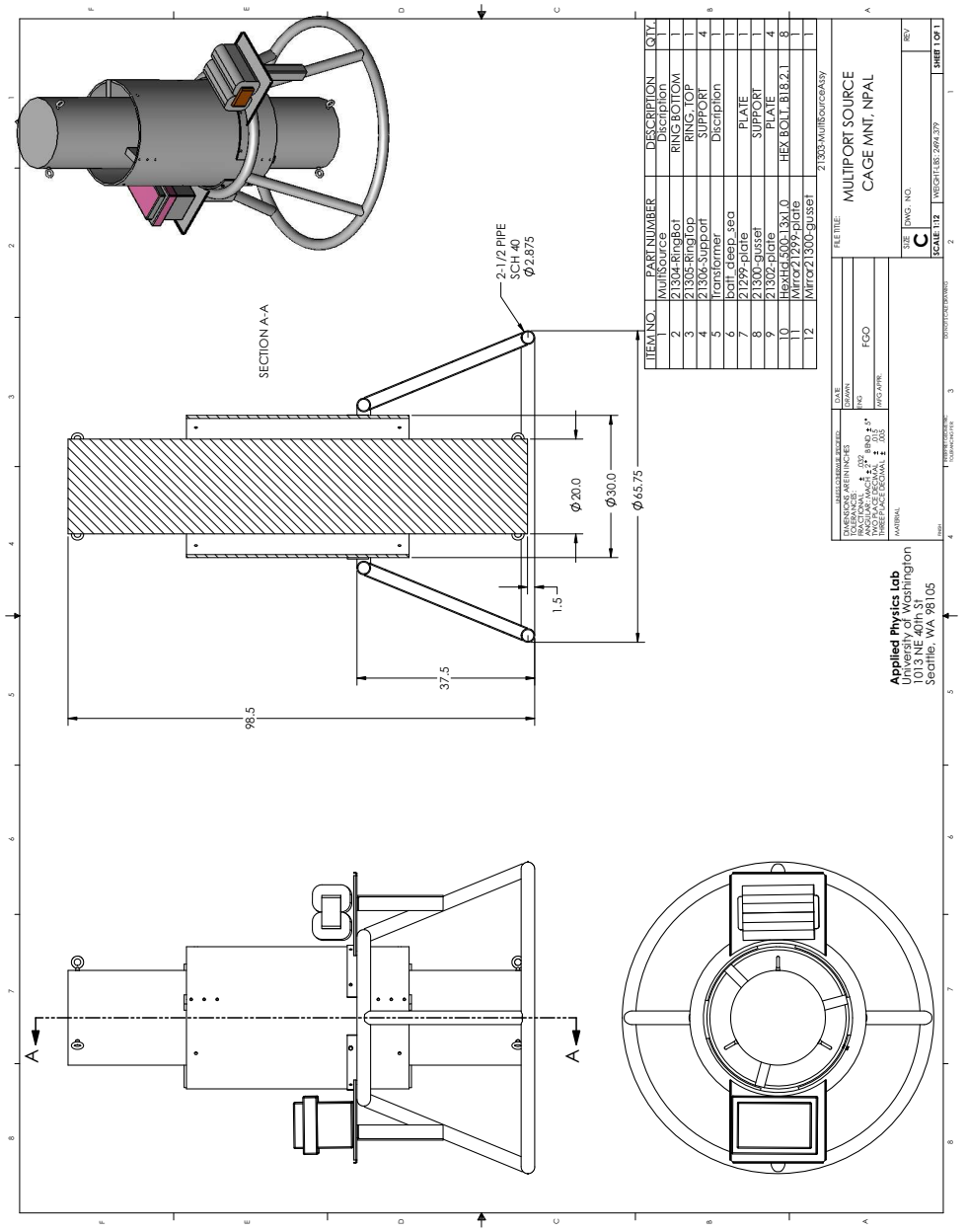

Figure 35: Engineering drawings, MP200/TR1446 assembly.

Figure 36: System fully assembled on the deck of the M/V *SeaHorse*, 2009 Lake Washington test.

Figure 37: Deck preparations, 2009 Lake Washington test.

Figure 38: Deployment from the M/V *SeaHorse*, January 2009 Lake Washington test. System fully assembled including sea battery, telemetry bottle, and tuner. Deployment and recovery utilized the barge's main crane. The lifting strap is attached to a hard point on the transducer; this was added based on an early lifting design. Once in the water, the system is transferred to the "electro-opto-mechanical" suspension cable, and is raised and lowered in the water via the APL-UW winch and suspension cable. In this picture, the suspension cable is only under mild tension. The block is also suspended from the main crane. The cable married for a short distance up the suspension cable is the monitor hydrophone cable (hydrophone not seen).

5 System Model

5.1 Introduction

The simple equivalent circuit model (section 2), which models only the electrical characteristics of the transducer, can be expanded to include all system components, from the input data file to the output radiated far field pressure. This provides a complete end-to-end modeling capacity. A block diagram of the system is shown in Fig. 39. Such a model requires the additional "transformation ratio" in the equivalent circuit model to transform from the electrical stage to the acoustical lumped equivalent circuit, in addition to elements for all other circuit components, such as the computer D/A, the power amplifier, etc.

5.1.1 D/A Converter

The D/A converter is one subsystem on the National Instruments NI PCI 6071E DAQ board. This is a 12-bit converter. The board uses the COMEDI driver, version 7.76. The conversion from input quanta to output voltage is set to 10 V/2048 quanta, or 4.88 mV per quanta.

Modeling this element requires only a simple scaling operation, where the scaling factor is 4.88 mV/quanta. This can be achieved very simply in a SPICE circuit with a 2-port network that drives a scaled version of the input "voltage" to the output port (Fig. 40). In this case, the input signal is not measured in volts but in D/A quanta.

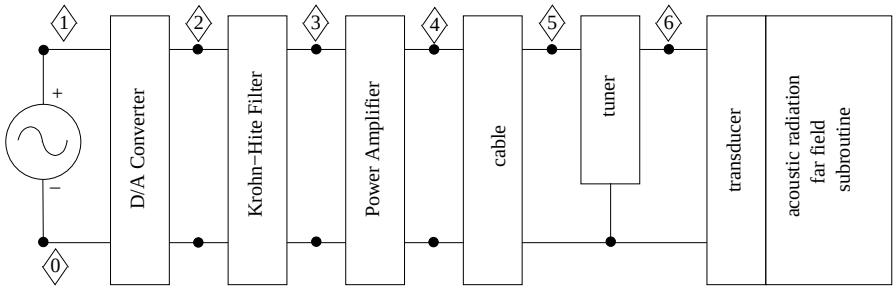

Figure 39: Block diagram of the entire system. The individual components are modeled as SPICE "subcircuits."

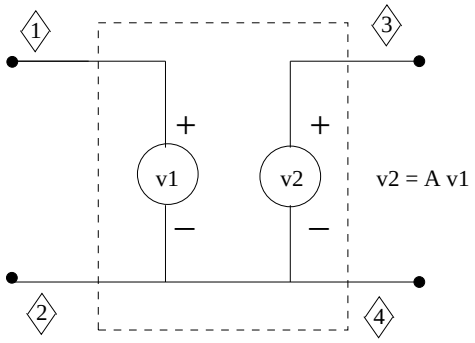

Figure 40: SPICE model for an ideal D/A converter. For this system, scale factor A is 4.88 mV/quanta. This is a generic model for all simple signal "scaling" operations that do not require fidelity of the input and output currents and impedances.

drive voltage [V RMS]	output voltage [V RMS]	ratio
2.40	621	258.8
2.74	708	258.4
3.09	799	258.6
3.44	889	258.4

Table 10: Input and output measurements for a 300-Hz sine wave, Instruments, Inc., L50 power amplifier. Source setting is *voltage source* with tap *1200/5.4*.

5.1.2 Power Amplifier

For simplicity, the power amplifier is modeled as a simple scaling factor, and therefore uses the same circuit as shown in Fig. 40.

The target power amplifier for at-sea experiments was an Instruments, Inc., [San Diego, CA] L50, modified for operation at low frequencies. The transfer function of the amplifier was measured at APL-UW using a sine wave generator for input, and a 500Ω resistor for a dummy load. Input signal RMS level was measured on a multimeter: amplifier output voltage RMS level was measured by a custom monitoring circuit. To a good approximation, the amplifier acts as a signal scaling element with a scale factor of 258 (Table 10).

5.1.3 Low-Pass Filter

To avoid a 175-Hz 4-pole low-pass Bessel filter built into the custom interface unit, the raw D/A output from the interface unit was used. This raw signal requires low-pass filtering

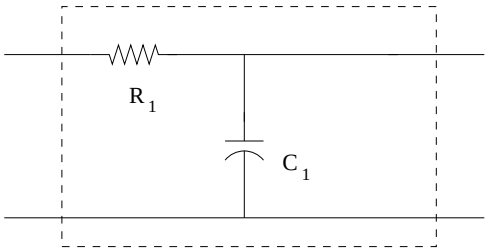

Figure 41: Circuit model for the low-pass filter.

element	value	comment
R_1	1 Ω	small, to minimize network loss
C_1	31.8 μF	to achieve a corner at 5000 Hz

Table 11: Circuit parameters for the low pass filter model.

to smooth out the staircase waveform output from the D/A. This was accomplished with a Krohn–Hite 3343 rack-mount filter. (A typical low-pass filter corner setting is 600 Hz on the Krohn–Hite filter.) A simple 1-pole *RC* (resistor–capacitor) network was used to crudely model the low-pass behavior of the filter (Fig. 41). Circuit element values are provided in Table 11.

5.1.4 Cable

Fred Karig (APL-UW) provided the cable parameters (Table 12). Fig. 42 shows the electrical model for the suspension cable.

5.2 Acoustic Radiation: the "Double Doublet" Model

A simple model for the acoustic radiation from a single tube (section 2.5) models the tube as an acoustic doublet. Extending this concept to the MP200/TR1446 produces a "double doublet" (Fig. 43). The radiation from each tube opening — the piston in the end of an unflanged (or partially flanged) pipe — is idealized as a monopole in free space. Let the

element	value	comment
R_{cable}	3.15 Ω	1.5 Ω/1000 ft from the manufacturer
C_{cable}	10.5 μF	25 pF/ft , using RG-8 specification

Table 12: Circuit parameters for the cable. Cable length is 4200 ft.

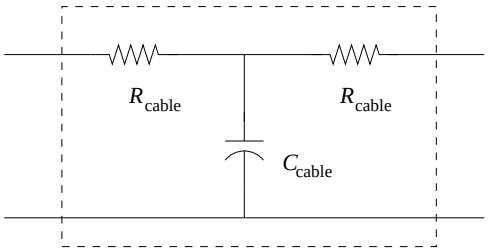

Figure 42: Circuit model for the cable.

acoustic particle velocity of the longer tube (lower frequency) be u_{LO} and that from the shorter tube (higher frequency) be u_{HI}. The Euclidean vector from the monopole to a field point is $\mathbf{r}_{\text{LO/HI}+/-}$, where the subscripted sign refers to the vertical position of the monopole.

The total far field pressure then utilizes the free space Green function from each monopole, and for a single frequency is given by

$$p(\mathbf{r}) = \Pi_{LO}\frac{e^{ikr_{LO+}}}{4\pi r_{LO+}} + \Pi_{HI}\frac{e^{ikr_{HI+}}}{4\pi r_{HI+}} + \Pi_{HI}\frac{e^{ikr_{HI-}}}{4\pi r_{HI-}} + \Pi_{LO}\frac{e^{ikr_{LO-}}}{4\pi r_{LO-}} \tag{27}$$

where the source level factors are given by (see Eq. 11)

$$\Pi_{LO,HI} = \pi a_{LO,HI}^2 \rho c k u_{LO,HI} \tag{28}$$

5.3 Model Implementation

The system model and the adjunct radiation routines were combined into a C++ program. The code generated the SPICE netlisting for the model, and initiated a call to SPICE to evaluate the circuit at multiple frequencies. A typical netlist is shown in Appendix B. The code then parsed the resulting SPICE output file to retrieve the transducer fluid velocities u_{LO} and u_{HI}. The code then used Eqs. 27 and 28 to compute the complex acoustic pressure response at each frequency at the desired field point. The code next multiplied the input signal spectrum by the complex acoustic pressure response at each frequency, and inverse Fourier transformed the result to a real time-domain signal. User-adjustable variables include the sound speed, the field point (x, y, z) in a coordinate system centered at the transducer, and the file name of the desired drive signal in `.wav` format.

A variety of predictions can be made with this model and code. Some examples follow.

5.4 Performance Validation

Because the RMS acoustic pressure at $[30.8, 0, 0]$ was used to relate $u_{LO,HI}$ to the transformation ratio S via Eqs. 17 and 8 via Eqs. 9 and 11 and a simplified version of the "double doublet" propagation model, the reverse calculation must hold: a sinusoidal input at 212 Hz should yield the measured RMS value at the field point. The measured RMS pressure was 8.64×10^6 μPa at RMS input current of 6.24×10^2 A (Table 5). (This current was measured at the top of the cable, but this will not introduce a significant error.)

The SPICE netlisting was altered to introduce a current sensing voltage source between the tuner and the transducer. Simple SPICE runs at the single frequency 212 Hz showed that a power amplifier factor of 8.83 produced the target RMS current for a v_{in} input with amplitude 100.

Next, the simulator code was modified to force the power amplifier scale factor to be 8.83, and the code exercised on an input file containing a sinusoid of frequency 212 Hz and amplitude 100 quanta. The output file at the field point $[30.8, 0, 0]$ was a simple sinusoid, and was read into Matlab where it was found to have an RMS value of 7.09×10^6, which is in error of 1.7 dB. This is adequate verification, considering all the approximations made in this simple transducer model.

5.4.1 Broadband Beampattern

The MP200/TR1446 is known to have a beampattern with non-negligible deviations from an omnidirectional pattern, particularly at the upper resonance frequency. An interesting relevant broadband computation is therefore the "beampattern" for an input m-sequence. Input signal file `m284.LW.eq.wav` was used for this calculation. This file contains an m-sequence with law 2033, Q of 2, carrier of 284.166666... Hz, and a sample rate of 8525 Hz. The amplitude was 170 quanta. The signal had been pre-equalized using the predicted equalizer filter (see section 6). A Matlab script was used to exercise the simulator at angles from 0° (i.e., broadside) to 90° (i.e., endfire) at a slant range of 100 m. At each angle, the script read the output time-domain file (in units of μPa) and computed the RMS value. The normalized beampattern is defined here as

$$B(\theta) = 20 \log_{10} \left(\frac{p_{\text{RMS}}(\theta)}{p_{\text{RMS}}(0^\circ)} \right) \tag{29}$$

Results show a drop of only a 4 dB in the broadband RMS levels from broadside to endfire (Fig. 44).

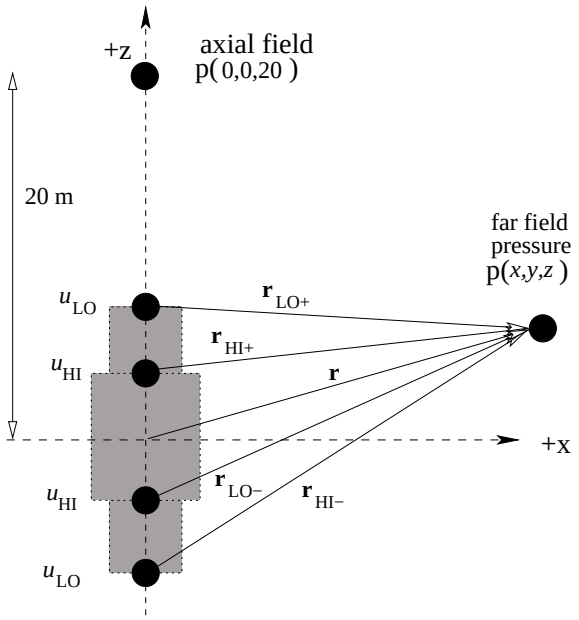

Figure 43: Geometry for the acoustic field computation. The radiated field is assumed to be axially symmetric around the transducer long axis. The axial field position at $(0, 0, 20)$ represents the monitor phone attached to the suspension cable.

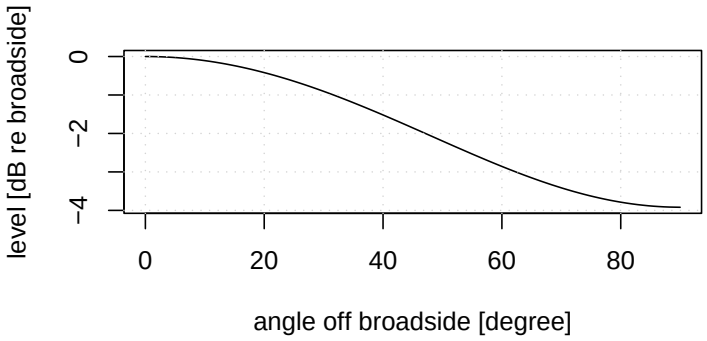

Figure 44: Theoretical broadband beampattern, based on a pre-equalized Q=2 m-sequence with carrier at $\approx$ 284 Hz.

5.4.2 Transmit Response

The full system model can be used to compute a transmit response similar to the standard transmit voltage response (TVR) used in transducer design. In this case, the transfer function is from the input `.wav` file (in units of "quanta") to output far field radiated pressure corrected back (via simple spherical spreading) to 1 m.

As an example, Fig. 45 shows the calculation for the entire system model for a far field broadside direction. This computation was performed using a Matlab script that looped through all frequencies; at each frequency, the script called a program to make a `.wav` file with 5 s of amplitude 100 sinusoid at the target frequency, called the simulator to propagate the field to the position $[100, 0, 0]$, and then read the resulting output file (which was a sinusoid in units of μPa) and computed its range-corrected RMS value. The response is this value normalized by the RMS amplitude of the input sinusoid, which is 70.71 quanta.

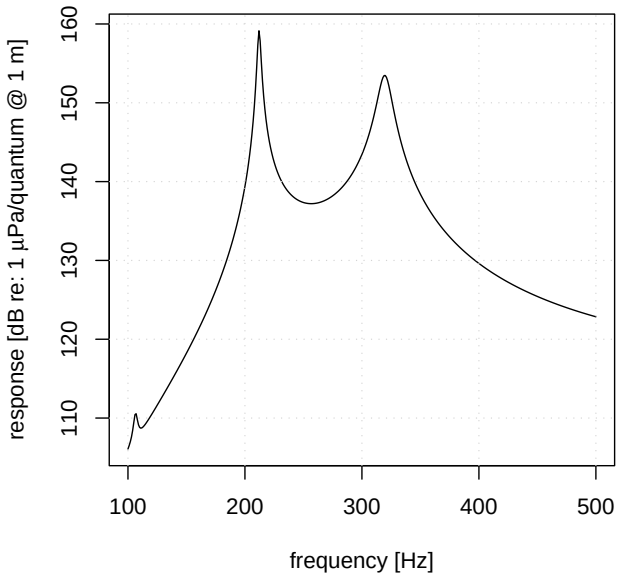

Figure 45: Theoretical transmit response based on the system model. Field location was $[100, 0, 0]$, i.e., 100 m at broadside. Input units are quanta, i.e., the exact `.wav` file values supplied to the D/A converter.

5.4.3 Broadside to Monitor Hydrophone Scaling

Transmit level monitoring during actual at-sea deployments will have only the monitor hydrophone available. Thus, it is desirable to devise a relationship between the broadband level measured at the location of the monitor hydrophone ($[0, 0, 21]$) and the broadside broadband source level corrected to 1 m. This is an easy computation to perform with the model. As an example, using the input file `m284.LW.eq.wav` and a sound speed of 1480 m/s yields an RMS pressure of 9.53×10^6 μPa at $[100, 0, 0]$ and 2.89×10^7 at $[0, 0, 21]$. The ratio $100p_{\mathit{field,RMS}}$ to $p_{\mathit{mon,RMS}}$ (range-corrected field RMS value to monitor RMS face-of-phone value) is 33.32, or 30.5 dB.

6 Signal Equalization

6.1 Introduction

The far field transfer function of the system is not flat across the two resonances, and this introduces considerable spectral shaping, typically undesirable, to any transmitted signal. To ameliorate this undesirable shaping, an "equalizer" was constructed by engineers at Massa Products, Inc. (Fig. 46). This unit was loaned to APL-UW in early 2008 under the terms of the tuner design contract with ImageAcoustics, Inc.

The transfer function of the Massa equalizer was measured on an HP3589A spectrum analyzer (Figs. 47 and 48). This measurement required the use of an auxiliary 80486 DOS machine configured with a National Instruments GPIB board to capture the trace to a DOS ASCII file (Table 13). The Massa equalizer would typically be inserted between the drive signal computer and the power amplifier (Fig. 49).

The use of the Massa equalizer has the advantage of simplicity: compensation for the spectral characteristics of the transducer is achieved by simply adding a hardware compo-

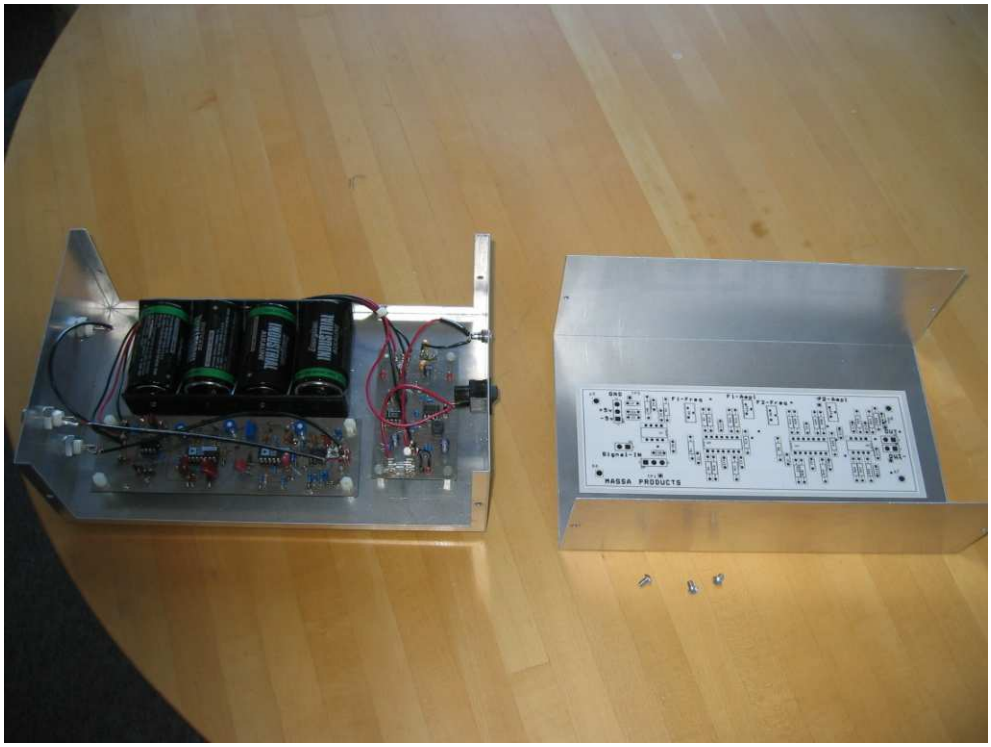

Figure 46: The Massa equalizer disassembled.

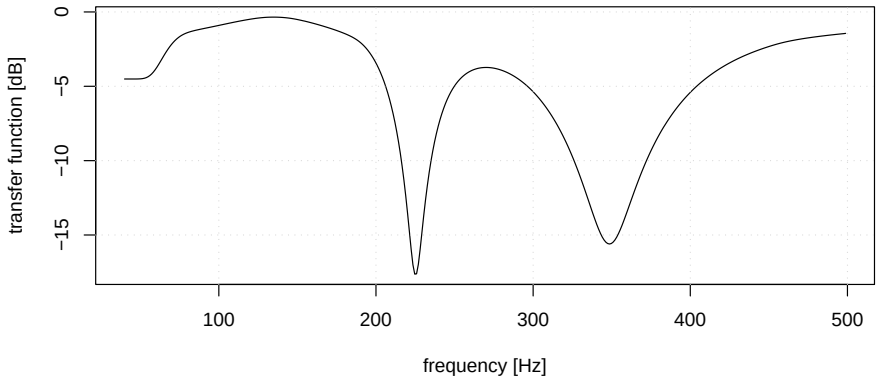

Figure 47: Magnitude response of Massa equalizer as measured on an HP3589 spectrum analyzer. Resolution bandwidth 1.1 Hz.

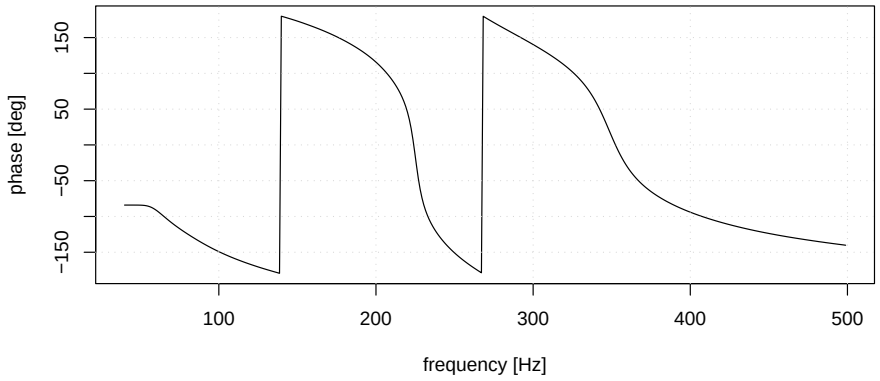

Figure 48: Phase response of Massa equalizer as measured on an HP3589 spectrum analyzer. Resolution bandwidth 1.1 Hz.

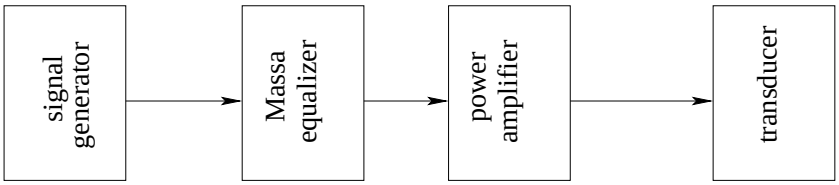

Figure 49: Schematic block diagram involving the Massa equalizer. (Tuner not shown).

command	purpose
`ibic`	starts the interactive session
`ibdev 0 19 0 13 1 0`	opens a device, connects to the analyzer
`ibwrt "DISP:RES D1"`	move trace in D1 register to trace A
`ibwrt "FORM:DATA ASC,7"`	set data format to ASCII, 7 sig. digits
`ibwrt "TRAC:DATA?"`	queues trace A data for retrieval
`ibrdf "FOO.DAT"`	transfers data from analyzer to DOS file
`ibonl 0`	closes the device

Table 13: AT-GPIB commands for retrieving trace data from the HP3589A.

nent into the signal circuit. The drawback of this approach is that the model for the entire system now requires a model for the Massa equalizer, which was not provided.

The alternative described below is to construct a "pre-equalizer" filter to pre-filter the drive signal. This filter is implemented in the frequency domain. The advantage is that the system model developed previously need not be modified, and, further, that the filter can be made to compensate nearly exactly for the hardware response (when SNR is high.) The disadvantage, primarily for the frequency domain filter, is that streaming operation of an original waveform through the filter is not possible without recourse to a more complex signal processing algorithm (such as an overlap-and-save methodology).

6.2 Theory

The equalizer filter can be developed using concepts from Wiener filter theory, where a signal X, after possibly passing through some signal conditioning, is received in the presence of additive noise N (Fig. 50). Let the acoustic field at the receiver be

$$P(\mathbf{r}) = XDGH(\mathbf{r}). \tag{30}$$

Therefore, the received signal is

$$Y(\mathbf{r}) = P(\mathbf{r})K + NK. \tag{31}$$

The optimal filter K_* is chosen to minimize the expected error between $Y(\mathbf{r})$ and $P(\mathbf{r})$. This gives

$$K_* = \frac{A|D|^2(HG(\mathbf{r}))^* S_{XX}}{|D|^2|HG(\mathbf{r})|^2 S_{XX} + S_{NN}} \tag{32}$$

where S_{XX} is the spectrum of the original input signal, S_{NN} is the autospectrum of the additive noise, and A is a user-adjustable scaling factor. Using simply $S_{XX} \rightarrow |X|^2$ and

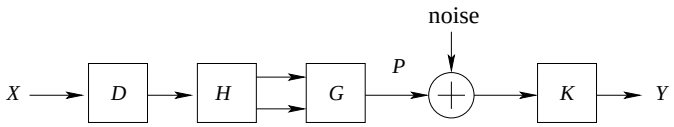

Figure 50: Signal flow diagram for a typical post-processing equalizer filter. D represents the D/A converter, the power amplifier, and the step-up part of the tuner. H represents the transducer, which is shown with two outputs, one for each pair of radiating tube openings. G is the Green function from both pairs of openings to a field point. K is a filter applied to the data received at a sensor at the field point. X is the input signal, P is the acoustic signal at the receiver. Y is the ultimate equalized output signal.

Eq. 30, one obtains

$$K_* = \frac{ADP^*(\mathbf{r})}{|P(\mathbf{r})|^2 + S_{NN}} \tag{33}$$

This is the equalizer transfer function.

In Wiener filter theory, K_* is computed from actual measurements of $P(\mathbf{r})$ and S_{NN}. Because the filter may depend on direction, the choice of $\mathbf{r}$ as the far field broadside direction would be appropriate, but it was not expected that measurements at such a location would be available during either calibration or actual field exercises. Therefore, a suboptimal approach was defined as follows. The quantity $P(\mathbf{r})$ was computed using the SPICE/C++ code, and the denominator in Eq. 33 was replaced by

$$|P(\mathbf{r})|^2 + S_{NN} \rightarrow |P(\mathbf{r})|^2(1+\epsilon) \tag{34}$$

where ϵ is a frequency-independent value that determines the contribution of the prediction $P(\mathbf{r})$ to the filter. ϵ is essentially the ratio of the noise to the signal. For ϵ much greater than 1, the output is dominated by the additive noise, and the filter mitigates the noise in the output by strongly attenuating components in X. For small ϵ, the output is dominated by the signal, and the filter essentially deconvolves out the factor $DHG(\mathbf{r})$. The choice here for ϵ is arbitrary in this suboptimal case.

All the filters in Fig. 50 are linear operators, and therefore can be applied in any order. The equalizer filter is therefore moved from its "post-acquisition" position in Fig. 50 to a position prior to the signal transmission equipment in Fig. 51. An off-line implementation of this arrangement is shown in Fig. 52.

To demonstrate the performance of the equalizer, a filter was developed for the system model described previously: this filter is known as file `eq01.nc`, with amplitude and phase characteristics shown in Fig. 53, and ϵ = 1000. Note the two deep nulls at the two transducer resonance frequencies, and the associated phase corrections.

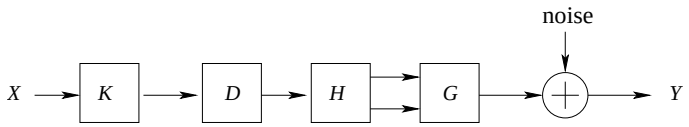

Figure 51: Similar to Fig. 50, but with the equalizer filter placed before the D/A converter.

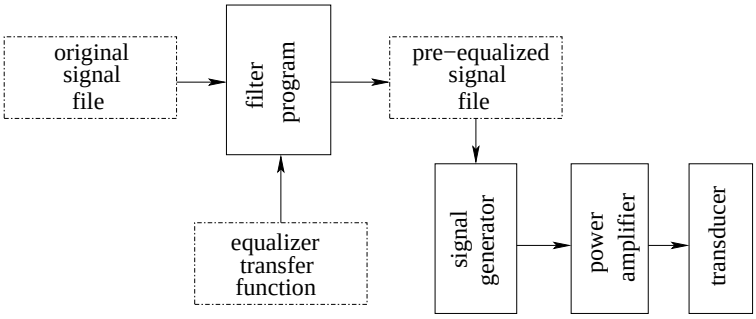

Figure 52: Off-line implementation of pre-equalization, based on Fig. 51.

An m-sequence with carrier frequency 300 Hz and a sample rate of 9600 Hz was processed through the system simulator and projected to a location of $[100, 0, 0]$, i.e., a broadside position at range 100 m. The signal at that location was pulse-compressed using a standard algorithm: the result is shown in the top panel of Fig. 54. This procedure was repeated for the same m-sequence pre-filtered by the transfer function in file `eq01.nc`: the result is shown in the bottom panel of Fig. 54. Without equalization, the single pulse, which would normally result from pulse compression, is distorted into multiple trailing pulses, but with equalization the pulse-compressed output contains a single prominent pulse.

Ideally, the best filter would use the actual drive signal and actual field location measurements.

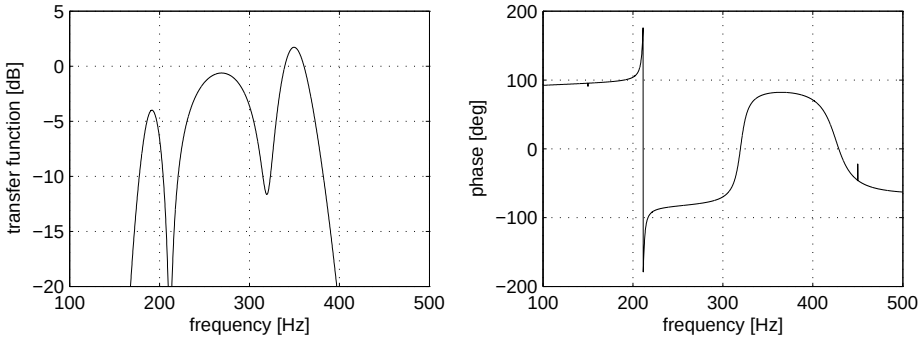

Figure 53: Equalizer transfer function, file `eq01.nc`

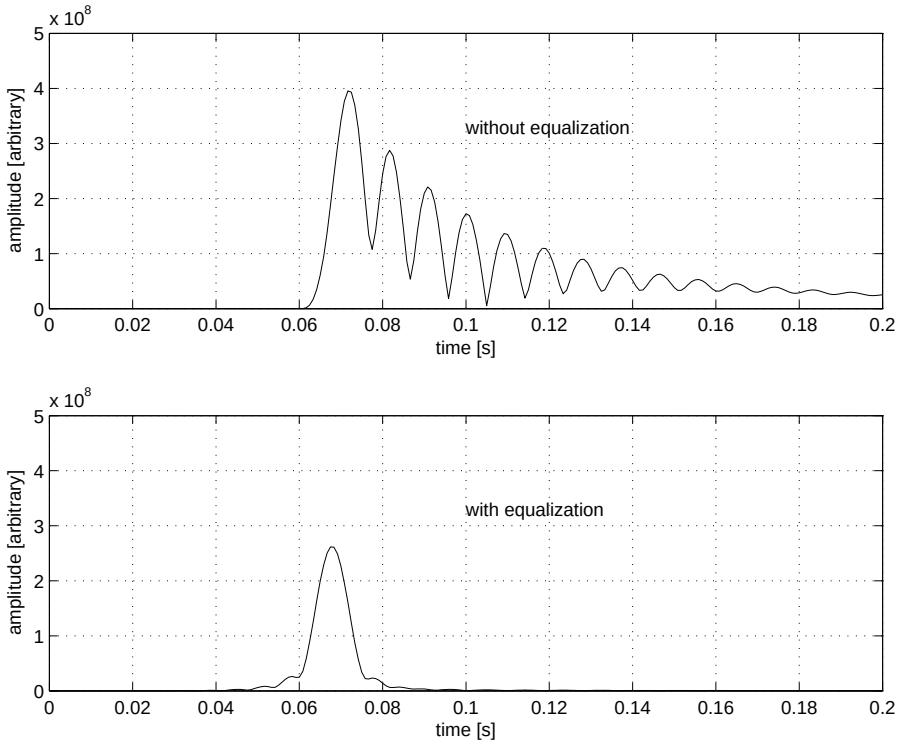

Figure 54: Pulse-compressed output without and with equalization. Simulated output at location [100,0,0]: direct path propagation delay at 1480 m/s is ≈ 68 ms.

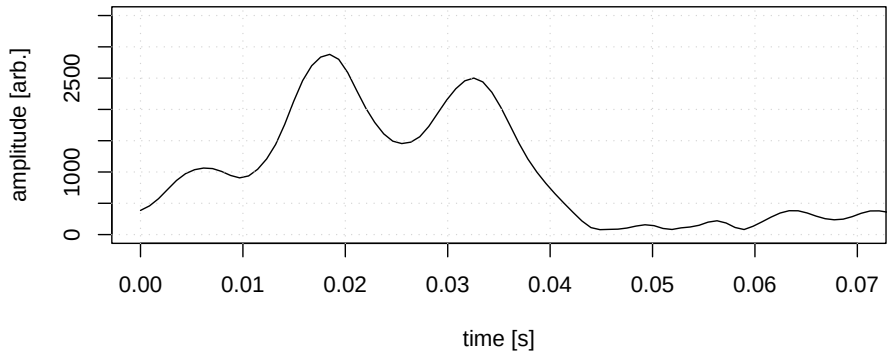

Figure 55: Pulse compressed noise signatures, 2009 Lake Washington test, from monitor hydrophone. Gain was code 5.

6.3 In-water Tests

The pulse-compressed signal from the monitor hydrophone acquired during a 2009 Lake Washington test is shown in Fig. 55. The record shows the direct path arrival, and the surface reflected path arrival. The MP200/TR1446 was at a depth of 30 m. A comparison of the acquired autospectrum and a predicted "signal-only" autospectrum is shown in Fig. 56: this computation includes the surface reflected arrival. There is reasonable correspondence between the predicted spectral shape and that visible above the background ambient noise, which was filled with harmonics from the ship's generators. Note that the nulls in the predicted spectrum do not fall exactly on the nulls observed in the radiated spectrum. This suggests that the equalizer based on the model is not quite accurate enough.

6.4 Summary

Pre-equalization based solely on the system model produced reasonable results during in-water tests. Sharp resonant peaks are observed both in the model and in the actual device; the sharpness of these peaks, however, makes accurate compensation difficult, as even a slight mis-tuning will place spectral minima off actual resonance. Such mis-tuning can be seen in the actual radiated signals.

Nevertheless, for the m-sequences used here, the pre-equalizer produces strong, well-shaped pulses (after pulse compression) with very low sidelobes.

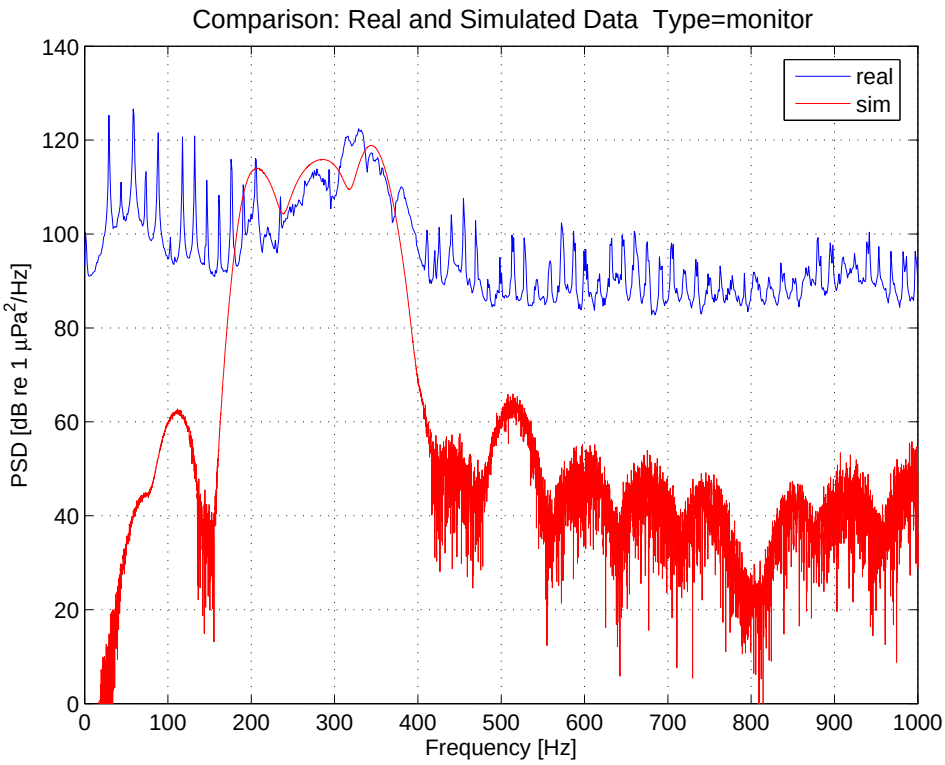

Figure 56: Real and simulated radiated spectra, 2009 Lake Washington test from monitor hydrophone.

Pre-equalizing a very long original waveform, or a streaming signal, would require a much more advanced algorithm. For such a case a post-signal generator hardware filter, i.e., the Massa equalizer, is probably simpler.

7 The Philippine Sea Engineering Test / Pilot Study

7.1 Summary

For several decades, the Office of Naval Research has sponsored an international consortium of scientists to investigate deterministic and stochastic acoustic propagation at low frequencies over long ranges in the deep ocean. Most of these "blue water" experiments have been conducted in the central North Pacific, where oceanographic processes are relatively benign. The natural progression for these studies is to determine whether and to what extent the models and predictions developed during these efforts apply in a region with more vigorous oceanic processes.

This scientific consortium identified the Philippine Sea as a reasonable venue for this effort. This region is bounded to the south by the North Equatorial Current (NEC) and to the west by the Kuroshio. Mesoscale structures propagate westward into the basin and collide with eddies spun off from the Kuroshio, creating energetic and complicated oceanography.

The primary scientific experiment is planned for 2010–2011, and involves a considerable number of new systems. To mitigate the risk of deploying new systems, the group conducted a pilot study/engineering test in the same operating environment in March–May 2009.

The geographical region of operations and the assets deployed are shown in Fig. 57. These include:

1. An autonomous transceiver mooring (T1). This unit was one of six under refurbishment for the 2010–2011 experiment, and was deployed at the design position for the T1 mooring.

2. A distributed vertical line array (VLA). In 2009 this was a 5000-m partially populated development version of a system targeted for the main experiment. This was located at the design intersection of two transects between several autonomous transceiver moorings scheduled for the 2010–2011 experiment.

3. Ship-suspended stationary operations along the path between T1 and the VLA. Stationary operations listed herein occurred at ship stops SS45 and SS107.

The MP200/TR1446 was freighted to Kao-Hsiung, Taiwan, in March 2009, and lifted aboard the R/V *Melville* for use during the ONR 2009 Philippine Sea engineering test / pilot study.

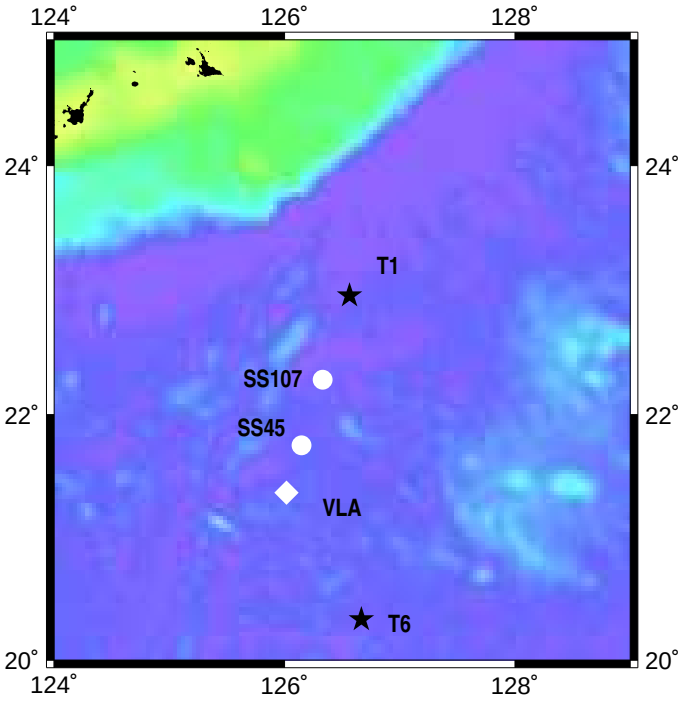

Figure 57: Geographical context for the Philippine Sea 2009 exercise. APL-UW deployed the MP200/TR1446 at ship stops SS45 and SS107.

Figure 58: Dockside mobilization, Kao-Hsiung harbor, April 2009. The MP200/TR1446 system was transported to Kao-hsiung in a softtop freight container.

The APL-UW multiport system was deployed four times during the 2009 exercise — three times at station SS45 (no transmissions were conducted during one of those deployments) and once at station SS107. A summary of transmissions is provided in Appendix C.

Although the 2009 Philippine Sea exercise was an engineering test of equipment, APL-UW also conducted an opportunistic program of high duty cycle full power transmissions to the Scripps VLA in between other activities. In total, the program netted 6.2 hours of cumulative transmission time out of 9.5 hours at station SS45, and 32.2 hours out of 60 hours at station SS107. A comprehensive analysis of those transmissions is the subject of future research.

7.2 System Limitations

How hard can the system be driven? Engineering measurements identified several constraints.

Figure 59: The MP200/TR1446 and the HX554 on the fantail of the R/V *Melville* prior to departure from Kao-Hsiung harbor. The SeaBattery and telemetry bottle are not yet attached to the MP200/TR1446.

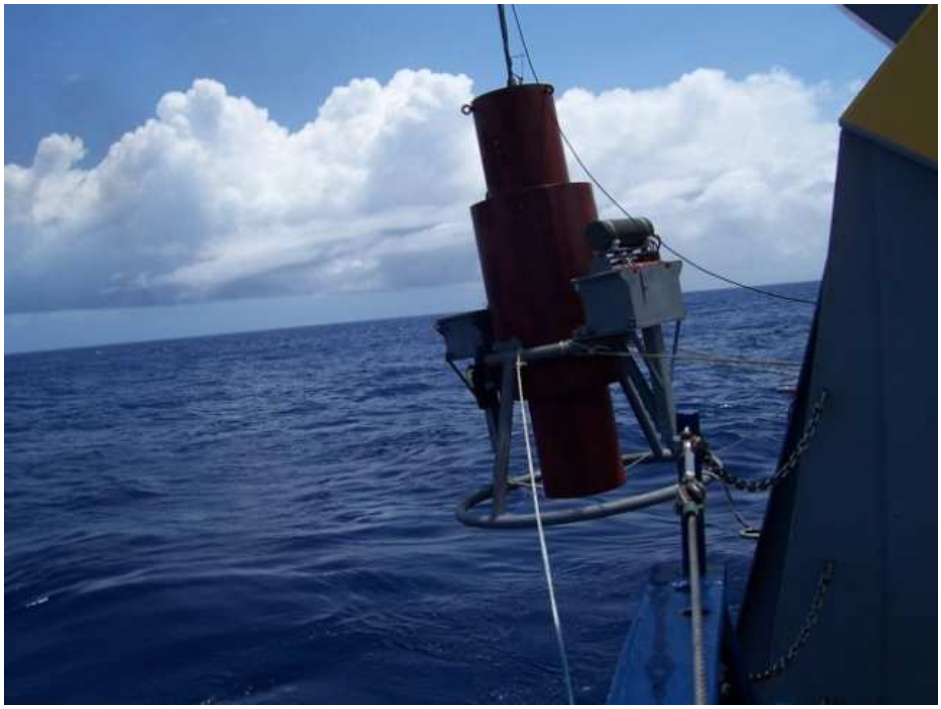

Figure 60: Deploying the MP200/TR1446.

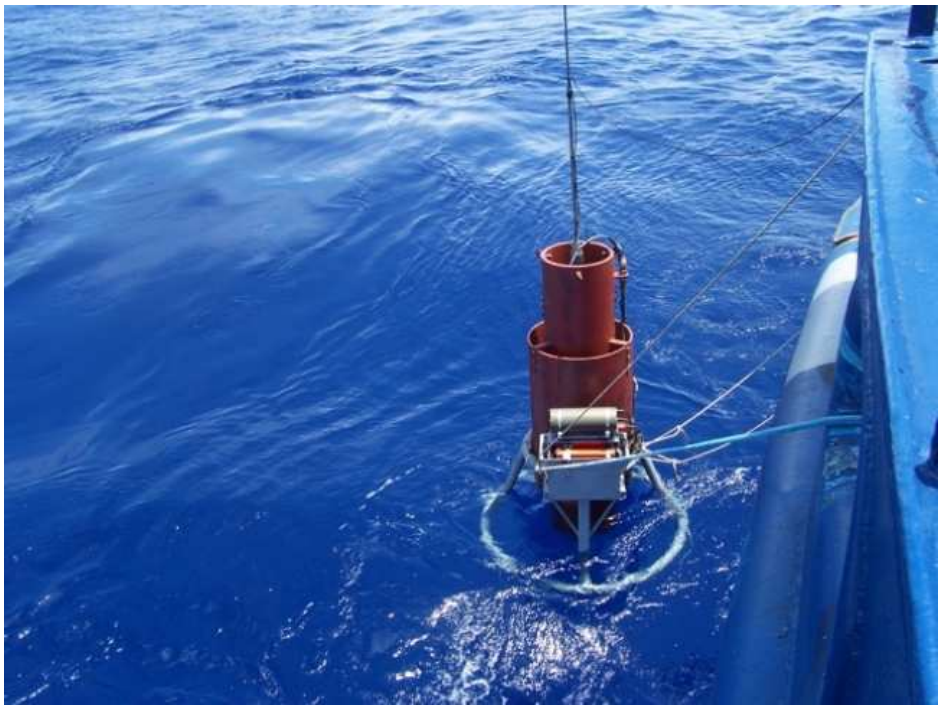

Figure 61: The MP200/TR1446 descending into the sea.

Figure 62: Recovering the MP200/TR1446. Two hand lines and two lines attached to air tuggers were used to control the system.

Figure 63: Attaching the monitor hydrophone and its bungy mounting frame to the suspension cable over the stern of the R/V *Melville* during deployment.

1. *Krohn–Hite Smoothing Filter*. Both sides of the Krohn–Hite filter were found to clip the positive side of an input waveform above about 8V; the negative side was good to -10V. This places an upper limit on the signal file amplitude at about 1500 quanta.

2. *Instruments, Inc., Amplifier*. The Instruments, Inc., L50 power amplifier was modified at APL-UW to convert 5 Vrms to 1200 Vrms on the voltage source setting 1200/5.4. This is the setting used to determine the conversion scale factor of 258 used in section 5. Using a maximum peak value of $1200 \times \sqrt{2}$ or 1697 V and a gain of 258, the maximum input peak voltage is 6.58 V, which corresponds to a peak signal file amplitude of 1348 quanta. This places a second, and more restrictive, limit on the input signal amplitude.

3. *MP200*. George Cavanagh of Massa advised, "The transducer should be used with the equalizer provided to ensure you do not overdrive the unit at the high Q peaks in the response. The Transmit Voltage Response (TVR) between the peaks appears . . . to be about 130 dB. A Sound Pressure Level (SPL) of 195 dB should be obtained at about 1800 V rms." [pers. comm., 10 October 2008] This corresponds to a peak voltage of 2550 V. Given the step-up autotransformer/tuner and the power amplifier gain, this corresponds to the most restrictive limit on input signal amplitude of 1011 quanta.

7.3 Lessons Learned

Several surprises were encountered with the multiport system during the Philippine Sea exercise.

- The difference between the theoretical and measured scaling between the monitor hydrophone and the source level was larger than expected. The theoretical value was given (section 5.4.3) as 30.4 dB, but the value measured in Lake Washington in January 2009 was 35.3.

- The radiated source levels were generally around 188.0 dB for the first few transmissions at station SS45 (see Appendix C), much less than predicted. The reason for the discrepancy remains unknown.

- The transmission levels dropped by about half a dB after the first few transmissions at station SS45, and remained there the rest of the station. The reason for this change also remains unknown.

- The seawater intrusion into the tuner housing caused irreparable damage to the tuner at station SS45. The work-around was to wire past the tuner, and drive the multiport

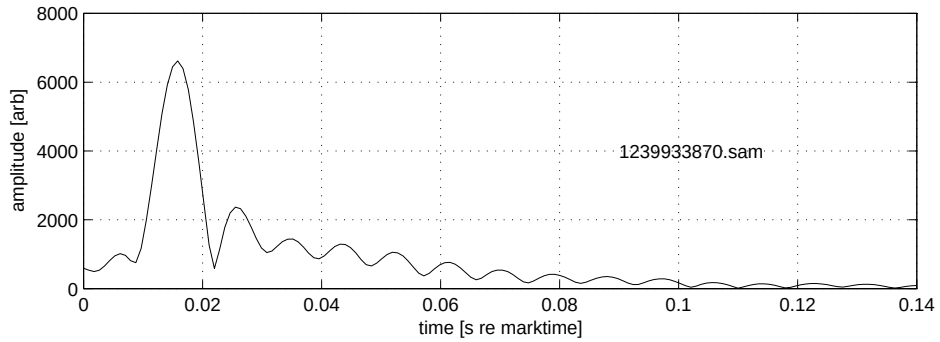

Figure 64: Pulse-compressed result, transmission file `1239933870.sam`, as measured on the monitor hydrophone.

transducer directly from the end of the EOM cable. This does not appear to have harmed the hardware. The loss of the 1:2 step-up tuner should have contributed to a 6 dB loss in radiated source level. Measurements based on the monitor hydrophone indicate that the levels were consistently about 182.5, or about 5 dB lower. Again, the discrepancy (here, of 1 dB) is not understood.

- The pulse-compressed waveforms from either the monitor hydrophone (Fig. 64) or from the vertical line array (not shown) suggest that the equalizer was not optimally tuned.

  As an example, consider the pulse-compressed output (Fig. 64) from the first full power transmission from SS45. The data are from file `1239933870.sam`, start time UTC 107:02:04:11. The data were captured on the monitor hydrophone, located vertically 21 m from the acoustic center of the MP200/TR1446. The propagation time over 21 m is approximately 14 ms: the pulse appears to arrive at about 16 ms, so this is the direct path. There was no detectable pulse in the record at the time expected for a surface-reflected path. (The depth was approximately 1000 m.) The pulse here has considerable trailing sidelobes, similar to but not as prominent as those in the uncompressed pulse example (Fig. 54).

  Suboptimal tuning can also be inferred from Fig. 56, which shows results from the 2009 Lake Washington test. In this figure, the nulls in the measured spectrum do not align with those in the theoretical spectrum. The "ringing" was not detected in the 2009 Lake Washington data because any "tail" behind the direct path pulse was obscured by the arrival of the surface-reflected pulse (see Fig. 55.)

  While there should exist some variation in the radiated signal spectrum from broadside to endfire, this variation remains unlikely to be the primary reason for the trailing sidelobes, and hence further refinements in the equalizer should be investigated.

It is no surprise that the performance predictions made with the system model were not completely accurate. Many simplifying approximations were made to establish the system model. Nevertheless, the discrepancies were not severe considering no full or even moderate power calibration was conducted with the fully assembled system. Without such a calibration, the effects on acoustic parameters such as resonance frequencies and broadside radiated source level of various system-level mechanical issues, such as the tuner mass and SeaBattery mass mounted at the transducer equator, remain unknown.

In spite of all the engineering approximations, the multiport system provided many hours of usable acoustic data during the 2009 Philippine Sea exercise. Further refinements are anticipated for future experiments.

References

[1] SPICE software is available for download from `http://embedded.eecs.berkeley.edu/pubs/downloads/spice/spice3f5.tar.gz`. This is the last official Berkeley release for Unix. The code was ported to and used under Linux.

[2] *Multiport Underwater Sound Transducer*, Butler, J.L., U.S. Patent Number 5,184,332, filed Dec. 6, 1990, dated Feb. 2, 1993.

[3] Butler, A.L., and J.L. Butler, "A Deep-Submergence, Very-Low Frequency, Broadband, Multiport Transducer," presented at the UDT Europe 2002 Conference, 19 June 2002.

[4] Butler, A.L., and J.L. Butler, "A Deep-Submergence, Very-Low Frequency Multiport Transducer", *Sea Technology*, Nov., 2003.

[5] Wilson, O.B., *Introduction to the Theory and Design of Sonar Transducers*, Peninsula Publishing, Los Altos, California, 198.

[6] Stansfield, D., *Underwater electroacoustic Transducers*, Bath University Press, 1991.

[7] Sherman, C.H., and J.L. Butler, *Transducers and Arrays for Underwater Sound*, Springer, 2007.

[8] Morse, P., and U. Ingard, *Theoretical Acoustics*, Princeton University Press, McGraw-Hill Co., 1989.

[9] Watson, J., "Power Amplifier Requirements for Driving the Alliant Bender Bar Projector to a 200 dB Source Level over 30 NM of SD Cable", memo to J. Mercer, dated 13 January 1993.

A 2006 Lake Washington Test Results

Twenty-one test measurements were conducted during the Lake Washington test of 2006. A summary of each collection is provided in Table 14.

Results of the admittance calculations for each transmission are shown only for the frequencies in $[100, 400]$ Hz. The admittance estimates outside this range were too noisy to be useful. Occasional frequency points are annotated on the figures themselves. The name of the data file is also provided in the figures.

file	start time (UTC)	depth
mptest01.sam	Apr 11 23:26:52 2006	Depth 150 ft
mptest02.sam	Apr 11 23:34:49 2006	Depth 150 ft
mptest03.sam	Apr 11 23:41:59 2006	Depth 150 ft
mptest04.sam	Apr 11 23:46:54 2006	Depth 150 ft
mptest05.sam	Apr 11 23:58:51 2006	Depth 150 ft
mptest06.sam	Apr 12 00:05:16 2006	Depth 150 ft
mptest07.sam	Apr 12 18:27:00 2006	Shallow
mptest08.sam	Apr 12 18:34:31 2006	Shallow
mptest09.sam	Apr 12 18:52:14 2006	Shallow, Law was 103, not used here
mptest10.sam	Apr 12 18:59:51 2006	Shallow, Law was 103, not used here
mptest11.sam	Apr 12 19:06:05 2006	Shallow
mptest12.sam	Apr 12 20:14:12 2006	Depth 100 ft
mptest13.sam	Apr 12 20:29:34 2006	Depth 100 ft
mptest14.sam	Apr 12 20:35:14 2006	Depth 100 ft
mptest15.sam	Apr 12 20:44:12 2006	Depth 100 ft
mptest16.sam	Apr 12 20:48:33 2006	Depth 100 ft
mptest17.sam	Apr 12 22:37:57 2006	Dockside, in air: garbage
mptest18.sam	Apr 12 22:43:55 2006	Dockside, in air: garbage
mptest19.sam	Apr 12 22:49:59 2006	Dockside, in air: garbage
mptest20.sam	Apr 12 23:09:36 2006	Dockside, 1 m deep : not used here
mptest21.sam	Apr 12 23:19:40 2006	Dockside, 1 m deep : not used here

Table 14: Summary of transmission collections, Lake Washington 2006 test. Most transmissions used an RMS drive voltage of about 100 V.

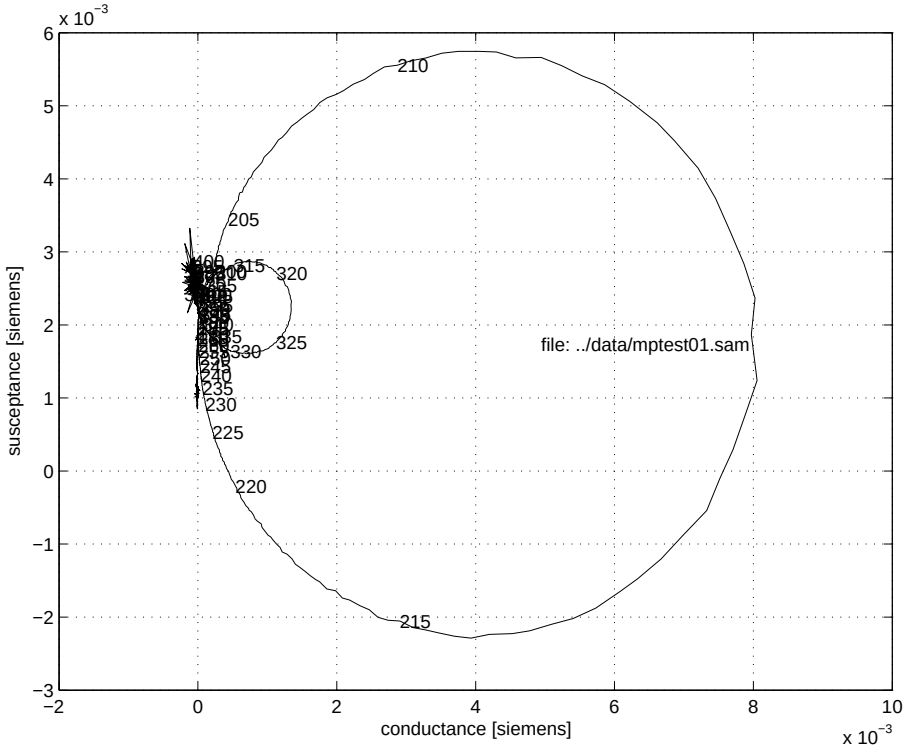

Figure 65: 2006 Lake Washington admittance loop, file `MPTEST01.DAT`

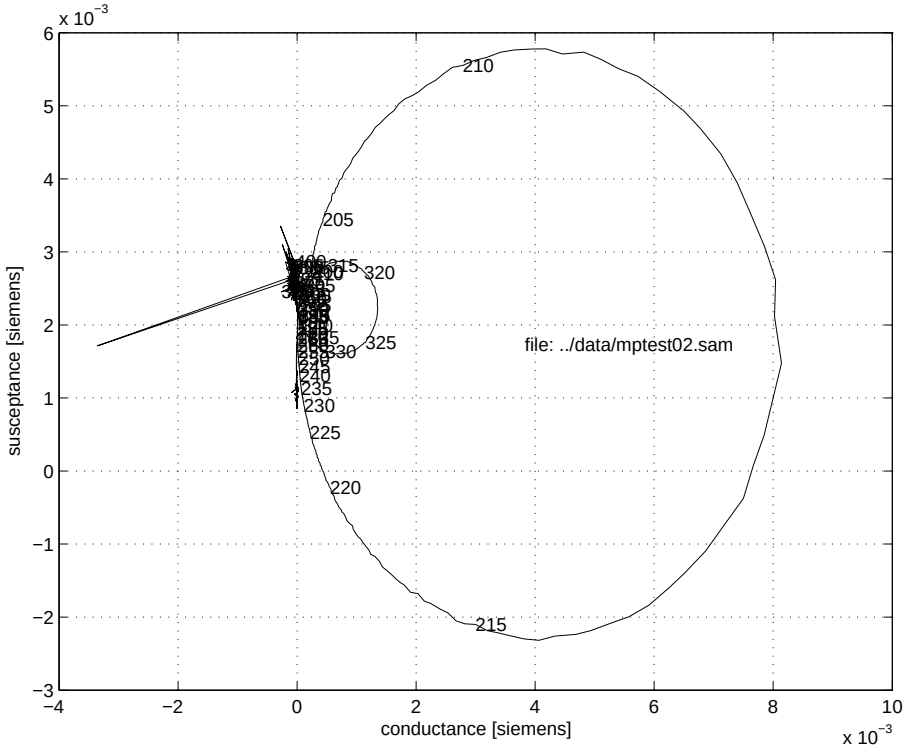

Figure 66: 2006 Lake Washington admittance loop, file `MPTEST02.DAT`

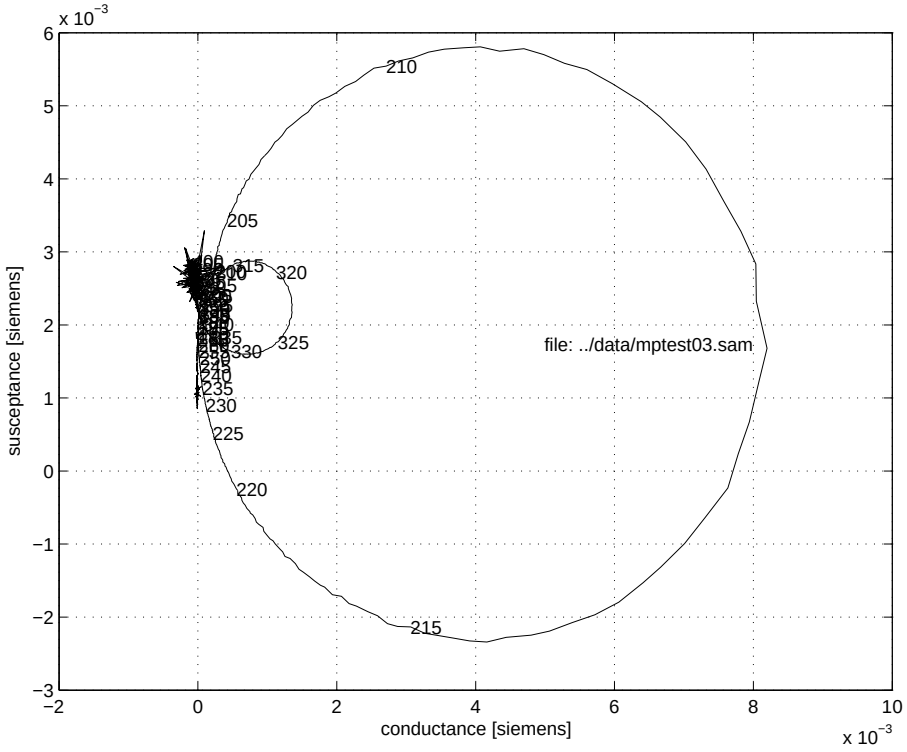

Figure 67: 2006 Lake Washington admittance loop, file `MPTEST03.DAT`

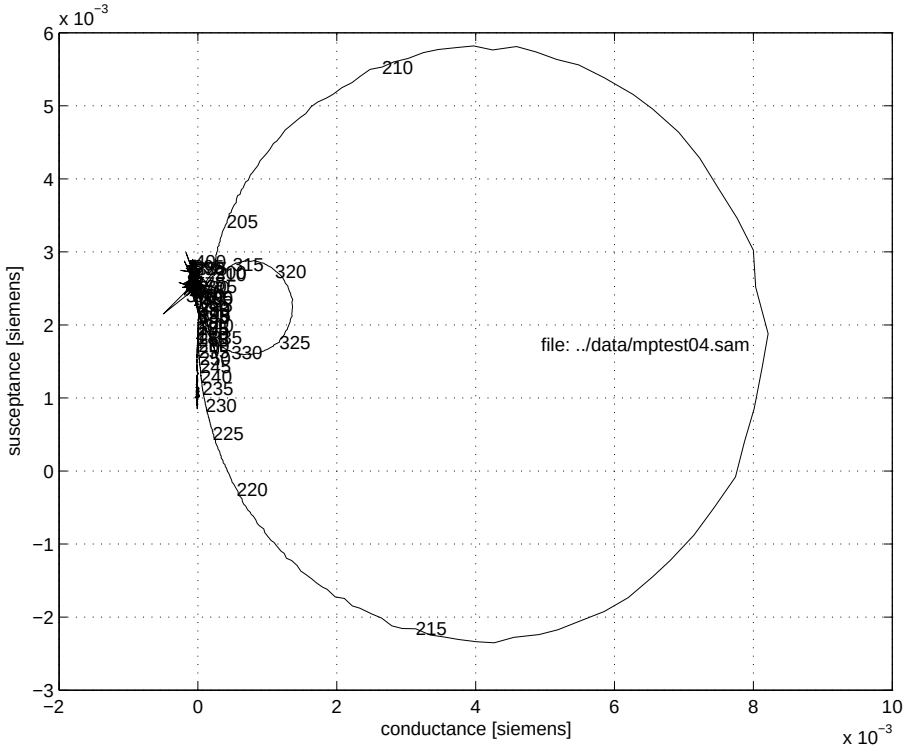

Figure 68: 2006 Lake Washington admittance loop, file `MPTEST04.DAT`

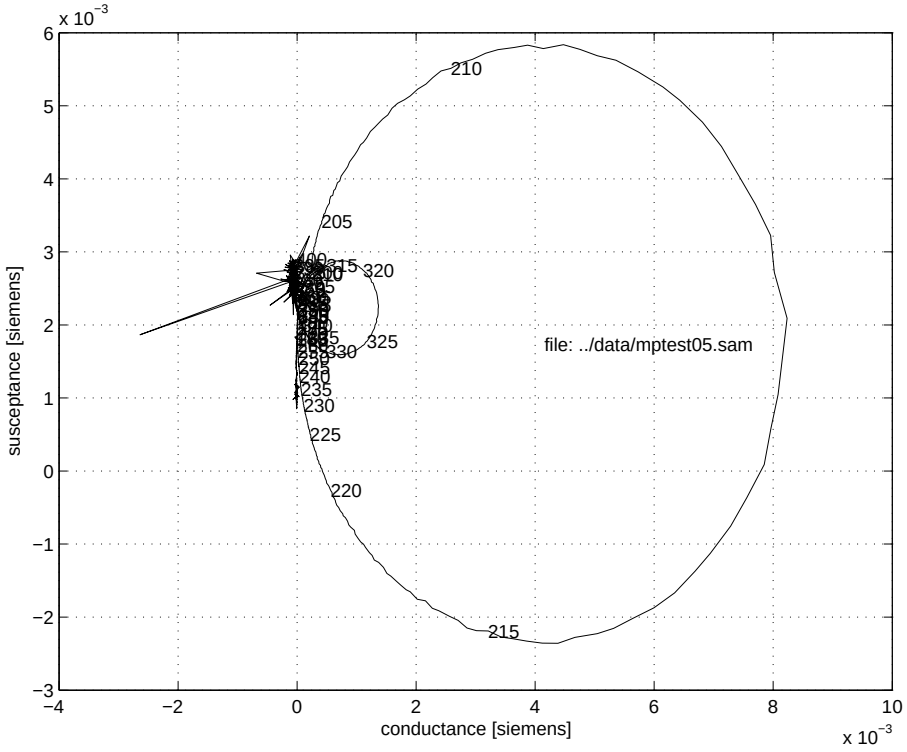

Figure 69: 2006 Lake Washington admittance loop, file `MPTEST05.DAT`

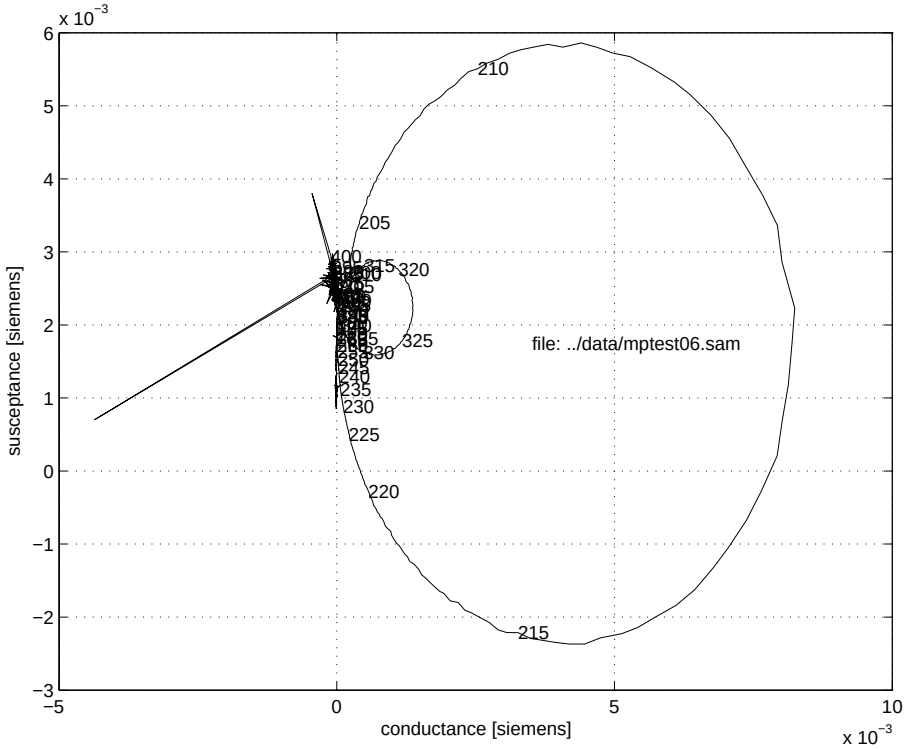

Figure 70: 2006 Lake Washington admittance loop, file `MPTEST06.DAT`

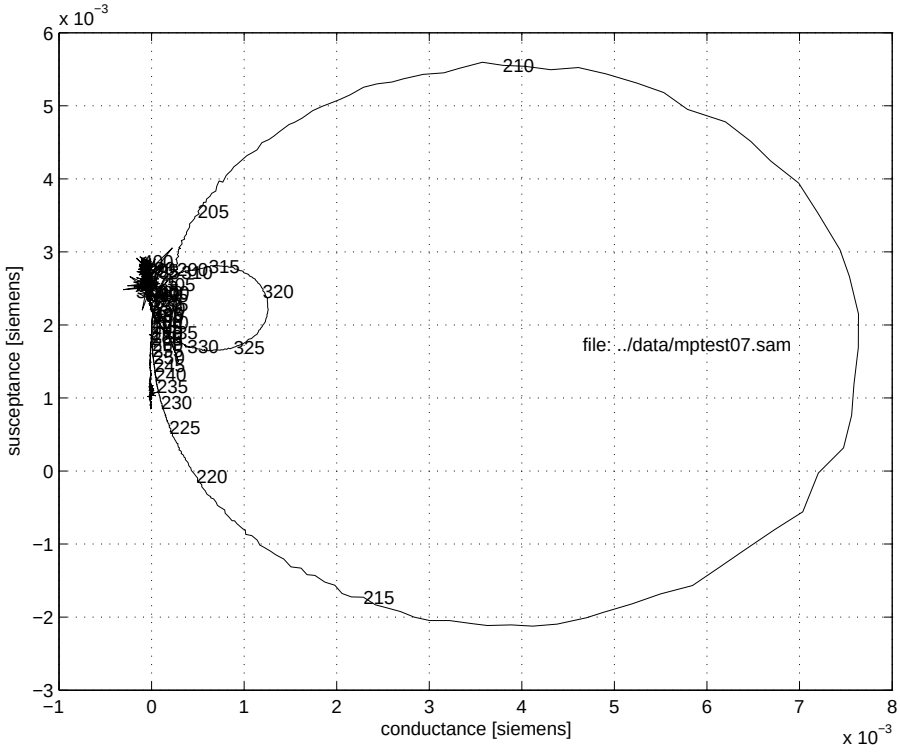

Figure 71: 2006 Lake Washington admittance loop, file `MPTEST07.DAT`

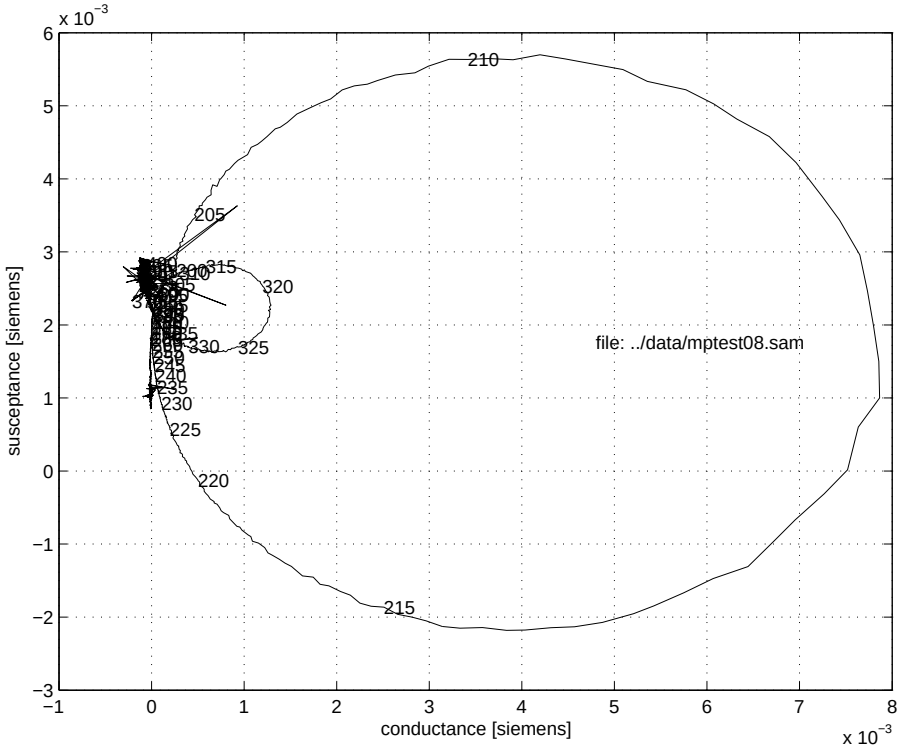

Figure 72: 2006 Lake Washington admittance loop, file `MPTEST08.DAT`

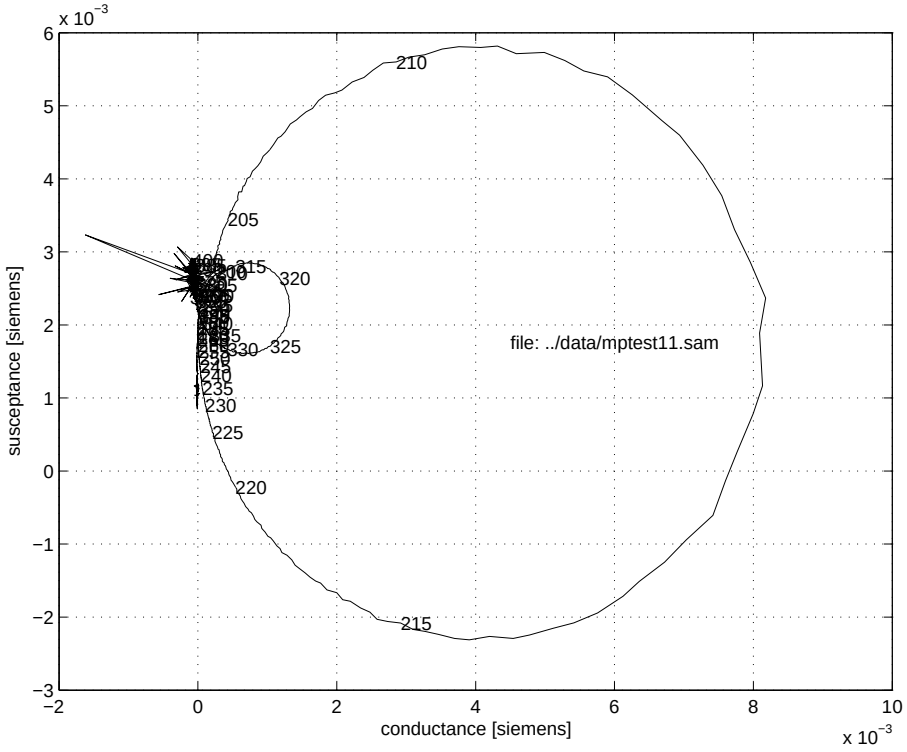

Figure 73: 2006 Lake Washington admittance loop, file `MPTEST11.DAT`

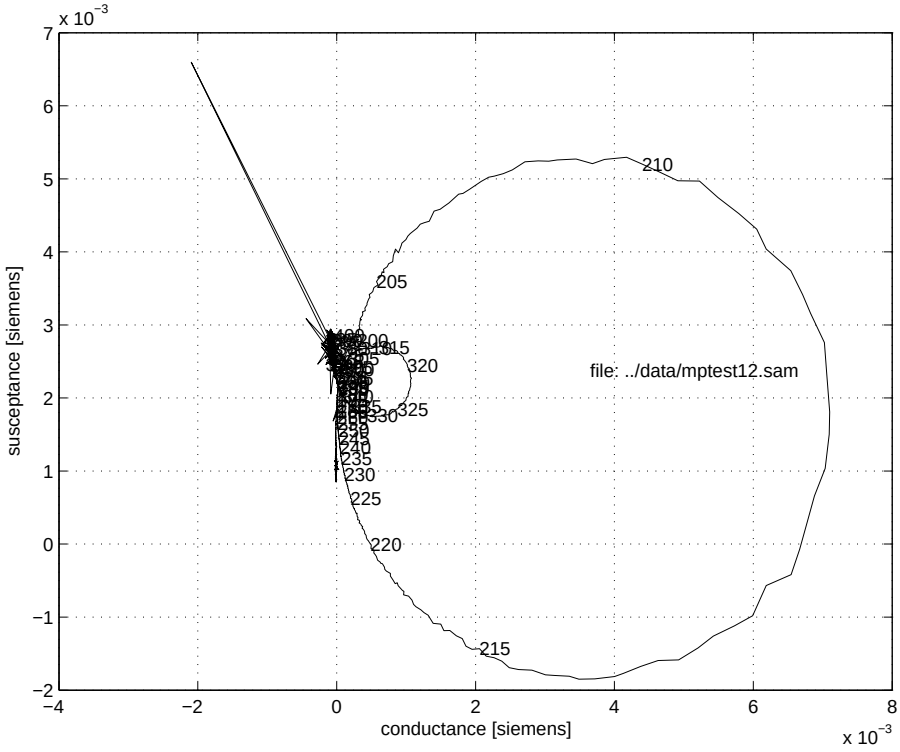

Figure 74: 2006 Lake Washington admittance loop, file `MPTEST12.DAT`

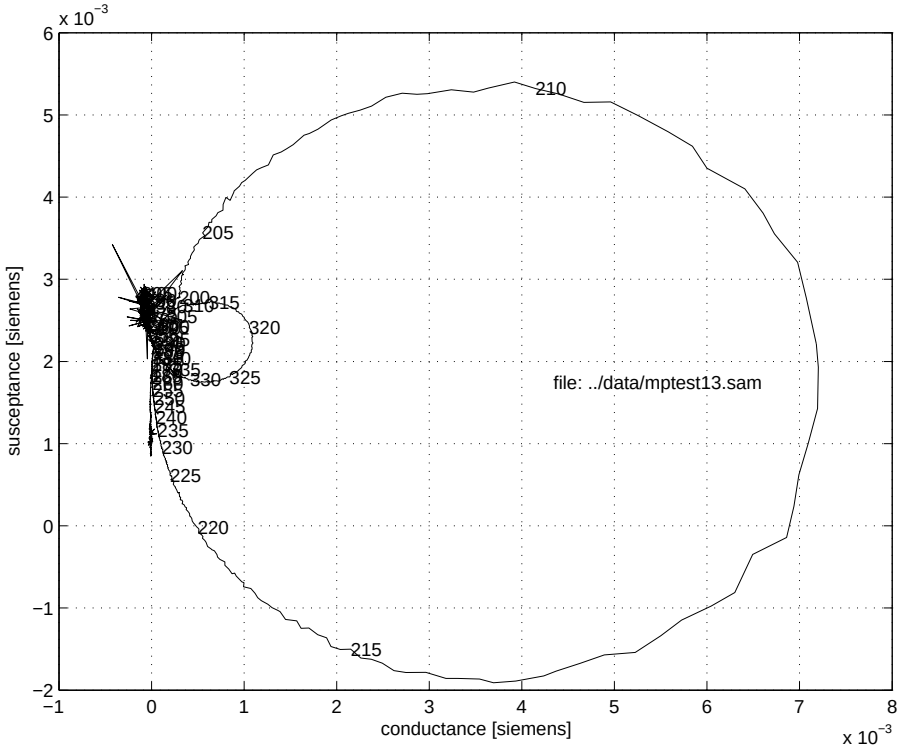

Figure 75: 2006 Lake Washington admittance loop, file `MPTEST13.DAT`

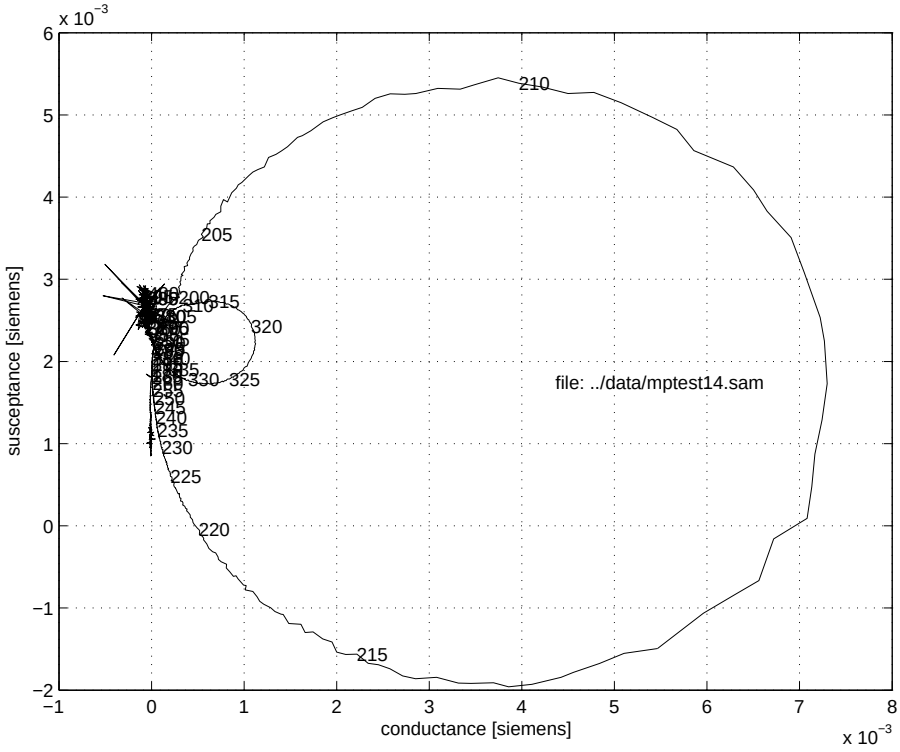

Figure 76: 2006 Lake Washington admittance loop, file `MPTEST14.DAT`

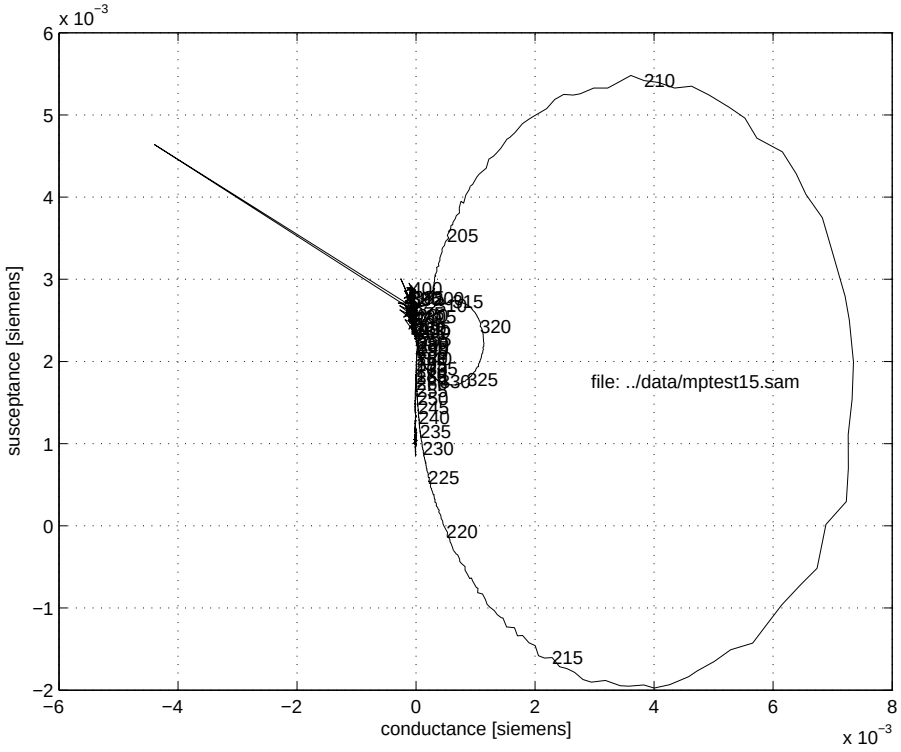

Figure 77: 2006 Lake Washington admittance loop, file `MPTEST15.DAT`

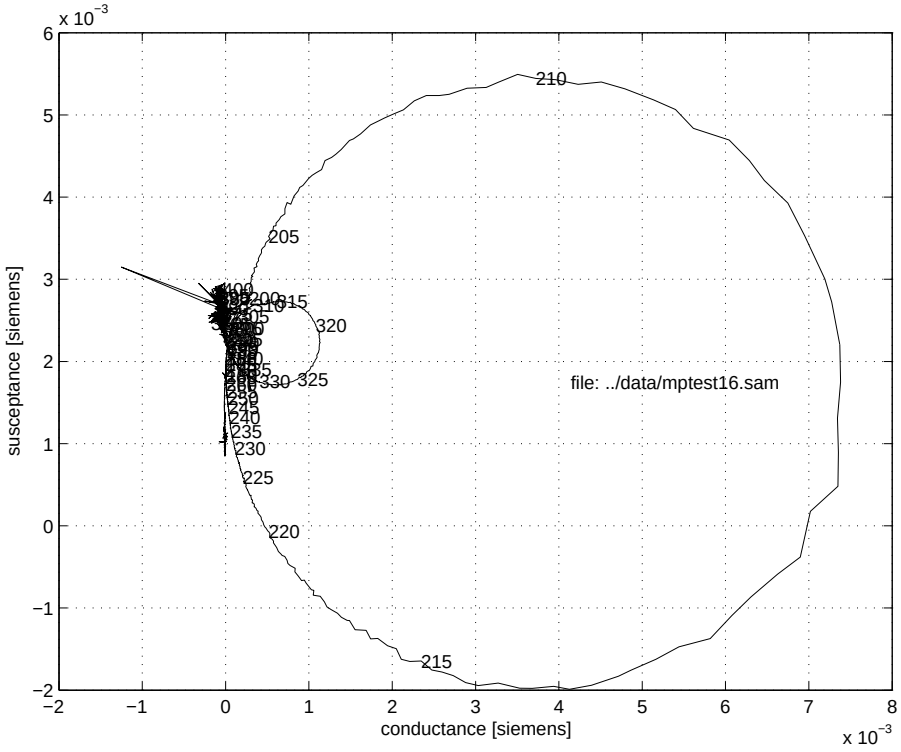

Figure 78: 2006 Lake Washington admittance loop, file `MPTEST16.DAT`

B System SPICE Netlist

The following netlist is the version generated automatically by the simulator.

```
automatic netlist, following TechMemo: 2009.08.01
******************************
******************************
* D/A subcircuit
.subckt DAconverter 1 2 3 4
rin 1 2 1e+06
eout 3 4 1 2 0.00488
.ends
******************************
* Krohn-Hite filter stand-in:
.subckt KrohnHiteFilter 1 2 3 4
rKH 1 3 1
cKH 3 2 3.18e-05
.ends
******************************
* L50 power amp:
.subckt PowerAmpL50 1 2 3 4
rin 1 2 1e+06
e1 3 4 1 2 258
.ends
******************************
* cable:
.subckt EOMcable 1 2 3 4
r1 1 5 3.15
r2 5 3 3.15
c1 5 2 1.05e-05
.ends
******************************
* tuner/autotransformer:
.subckt CoiltronTuner 1 2 3
lp1 3 5 0.15
rp1 5 1 1
lp2 1 6 0.15
rp2 6 2 1
kcoupling lp1 lp2 0.98
.ends
******************************
* transducer MP model, S = 8.12e4
```

```
.subckt MPtransducer 1 2 3 4 5
c0 1 2 1.25e-06
f1 1 2 vsensea -1.23e-05
e1 6 5 1 2 1.23e-05
vsensea 6 7 dc 0
clo 7 8 712
llo 8 9 7.92e-10
rlo 9 3 1.93e-08
chi 7 10 181
lhi 10 11 1.37e-09
rhi 11 4 1.06e-07
.ends
******************************
* circuit:
vin 1 0 ac 1.00 dc 0.0
x1 1 0 2 0 DAconverter
x2 2 0 3 0 KrohnHiteFilter
x3 3 0 4 0 PowerAmpL50
x4 4 0 5 0 EOMcable
x5 5 0 6 CoiltronTuner
x6 6 0 7 8 0 MPtransducer
vsenselo 7 0 dc 0
vsensehi 8 0 dc 0
******************************
.ac lin 12499 0.2 2499.8
.options NOPAGE
.print ac i(vsensehi)
.end
```

C 2009 Philippine Sea Transmissions

C.1 Background

Signals were transmitted during the 2009 ONR Philippine Sea Pilot Study/Engineering Test at two "ship stops," SS45 and SS107. The total number of multiport system transmissions at stations SS45 and SS107 were 19 and 214, respectively. The respective total transmission times were 6.2 hours spanning 9.5 hours and 32.3 hours spanning 60 hours.

A transmission file was generated for each transmission. The start time is given in the form YYY:HH:MM:SS where YYY is the yearday with January 1 being 001, all in UTC. The times listed below are the actual times of the first second of transmission, as decoded from the IRIG channel. The marktime is 20 seconds later, and may be different by 1 second from the target marktime recorded in the file header. (See below for explanation.) The ramp in all cases is 20 seconds.

C.2 Station SS45

There were three deployments of the MP200/TR1446 at SS45:

1. From 4/17 00:00Z to 4/18 00:00Z (day 107). Scheduled transmissions were interrupted several times for heat build-up issues in the science van. Transmissions were aborted due to shorting in the underwater package. This was later determined to be due to seawater in the transformer housing (oil expansion system tubing disconnected, possibly in going through the air–sea interface in strong currents.)
2. From 4/20 02:00Z to 4/20 08:00Z (day 110). The second transmission was aborted due to shorting in the underwater package. This was later determined to be a leak in the splice: there was also possible damage to the autotransformer.
3. 4/24 (day 114). The MP200/TR1446 was deployed, and stopped at about 200 m for a check, but it was determined that the underwater package was shorted. It was recovered, and the autotransformer was found to be shorted. No transmissions resulted from this deployment.

The signal file in all cases was `m284.EQ.wav`, with parameters given in Table 15. Transmissions are listed in Table 16.

The system time was observed to be drifting relative to the local GPS and ship NTP time servers. The reason for the drift is unknown as it was not observed in the laboratory

carrier	284.166666 Hz
cycles/digit	2
digit length	7.04 ms
sequence length	1023
law	2033
filtering	eq01.nc

Table 15: Signal parameters, 2009 Philippine Sea experiment.

at APL-UW. The two time servers did not differ by more than 100 ms, generally much less. The effect of this drift is that the actual transmission time may be the second adjacent to the desired start time: the transmission program (which was reading the system clock) triggered on the desired second as read from the system clock, but the hardware (which was synchronized by the local GPS) was on a different second, i.e., based on cruise hindsight, the GPS second was in fact the desired second, and the time read from the system clock was incorrect. At no time during occasional checks and subsequent testing was it ever observed that the GPS lost lock.

Table 16: Multiport transmissions for station SS45 in the 2009 Philippine Sea experiment. Duration includes ramp.

file name	start time [UTC]	duration [s]	source level	comments
1239933870.sam	107:02:04:11	3046.2	188.1	off by 1 second
1239937038.sam	107:02:56:58	253.3	188.0	
1239937470.sam	107:03:04:10	647.5	188.1	Aborted
1239941070.sam	107:04:04:10	3047.2	188.2	
1239944238.sam	107:04:56:58	253.3	187.8	
1239951438.sam	107:06:56:58	252.0	190.9	Sample rate error
1239951870.sam	107:07:04:10	3033.3	190.9	Sample rate error
1239955038.sam	107:07:56:59	252.5	187.7	off by 1 second
1239955470.sam	107:08:04:11	3046.5	187.8	off by 1 second
1239958638.sam	107:08:56:59	252.5	187.6	off by 1 second
1239959070.sam	107:09:04:11	3046.2	187.7	off by 1 second
1239962238.sam	107:09:56:59	253.2	187.5	off by 1 second
1239962670.sam	107:10:04:10	3047.2	187.8	
1239965838.sam	107:10:56:59	253.2	187.7	off by 1 second
1239966270.sam	107:11:04:10	1381.0	187.3	aborted
1240203438.sam	110:04:56:58	253.3	187.5	
1240203870.sam	110:05:04:11	3046.2	187.6	off by 1 second

continued on next page

file name	start time [UTC]	duration [s]	source level	comments
1240207038.sam	110:05:56:59	252.5	187.4	off by 1 second
1240207470.sam	110:06:04:11	3020.8	187.5	off by 1 second, aborted

C.3 Station SS107

The MP200/TR1446 was deployed at station SS107 from about 4/27 01:30Z (day 117) to about 4/29 16:00Z (day 119). The autotransformer was electrically disconnected in the underwater package, and the power amplifier signal was essentially driven directly into the MP200/TR1446.

Initial tests at depth indicated that the multiport itself would only require about 1.6 A rms at the maximum drive voltage, so we felt more confident that heat build-up would not be a problem. Therefore, we scheduled the source using the file `m284.EQ.wav` on the normal long/short schedule. This worked for about 2 hours, but then we experienced two failures. The first was a change in cable voltage and current, along with a corresponding increase in radiated power. This was likely due to a shift in D/A trigger clock frequency. Both the time board and GPS were replaced by backup units. The other problem was sporadic fault conditions on the power amplifier. This problem might last only one period, or many seconds. The only known corrective procedure at the time was to give the cabinet a shake and hope for the best. (This worked 3 times out of 3.)

Occasionally a transmission was aborted manually when a fault came on. These are noted below. Nevertheless, based on the notion that these faults were exacerbated by heat build-up, the transmission schedule was changed to one closer to a 50% duty cycle. To avoid complete transmission down time while the new schedule was being recalculated and verified, several 10-minute transmissions were launched manually. These are unlikely to be synchronized to the original m-sequence schedule, and are labeled “disparate” in Table 17.

This new automatic schedule, utilizing 35 transmission minutes per hour, began around 10:00Z on day 117 (4/27). This schedule ran 10 min on 5 off, 10 on 5 off, 15 on 15 off per hour. This schedule was used throughout the night.

At approximately 01:00Z on 118 (4/28) the schedule was modified to add 150 seconds of transmission data at the top of the hour. This was primarily to get a burst of measurements in the otherwise long gap starting about 48 minutes after the hour.

Amplifier glitches were occasionally observed by watchstanders: these lasted from one period to several seconds or more. The files have not been cleansed of any consequent

waveform interruptions, and the locations of such anomalies remain to be determined from the files themselves.

Table 17: Multiport transmissions for station SS107 in the 2009 Philippine Sea experiment. Duration includes ramp.

file name	start time [UTC]	duration [s]	source level	comments
1240804596.sam	117:03:56:16	253.3	182.8	
1240805028.sam	117:04:03:28	3047.3	182.9	
1240808196.sam	117:04:56:16	253.3	182.7	
1240808628.sam	117:05:03:28	3047.3	182.9	
1240811796.sam	117:05:56:16	251.2	185.8	samplerate error
1240812228.sam	117:06:03:28	3023.6	185.8	samplerate error
1240815396.sam	117:06:56:16	251.2	185.6	samplerate error
1240815828.sam	117:07:03:28	765.8	185.6	samplerate error, aborted?
ss107-disparateA.sam	117:08:22:43	621.3	N/A	manual launch
ss107-disparateB.sam	117:08:34:02	621.3	N/A	manual launch
1240822596.sam	117:08:56:16	253.3	182.7	
1240823028.sam	117:09:03:28	1271.8	182.5	aborted
ss107-disparateC.sam	117:09:27:27	621.3	N/A	manual launch
1240826628.sam	117:10:03:28	621.3	182.7	
1240827528.sam	117:10:18:28	621.3	182.7	
1240828428.sam	117:10:33:28	921.3	182.7	
1240830228.sam	117:11:03:28	621.3	182.7	
1240831128.sam	117:11:18:28	621.3	182.7	
1240832028.sam	117:11:33:28	921.3	182.7	
1240833828.sam	117:12:03:28	621.3	182.7	
1240834728.sam	117:12:18:28	621.3	182.7	
1240835628.sam	117:12:33:28	921.3	182.7	
1240837428.sam	117:13:03:28	621.3	182.7	
1240838328.sam	117:13:18:28	621.3	182.7	
1240839228.sam	117:13:33:28	921.3	182.8	
1240841028.sam	117:14:03:28	621.3	182.6	
1240841928.sam	117:14:18:28	621.3	182.7	
1240842828.sam	117:14:33:28	921.3	182.7	
1240844628.sam	117:15:03:28	621.3	182.7	
1240845528.sam	117:15:18:28	621.3	182.7	
1240846428.sam	117:15:33:28	921.3	182.7	
1240848228.sam	117:16:03:28	621.3	182.7	

continued on next page

file name	start time [UTC]	duration [s]	source level	comments
1240849128.sam	117:16:18:28	621.3	182.7	
1240850028.sam	117:16:33:28	921.3	182.7	
1240851828.sam	117:17:03:28	621.3	182.6	
1240852728.sam	117:17:18:28	621.3	182.6	
1240853628.sam	117:17:33:28	921.3	182.6	
1240855428.sam	117:18:03:28	621.3	182.6	
1240856328.sam	117:18:18:28	621.3	182.6	
1240857228.sam	117:18:33:28	921.3	182.6	
1240859028.sam	117:19:03:28	621.3	182.6	
1240859928.sam	117:19:18:28	621.3	182.6	
1240860828.sam	117:19:33:28	921.3	182.7	
1240862628.sam	117:20:03:28	621.3	182.8	
1240863528.sam	117:20:18:28	621.3	182.7	
1240864428.sam	117:20:33:28	921.3	182.7	
1240866228.sam	117:21:03:28	621.3	182.7	
1240867128.sam	117:21:18:28	621.3	182.7	
1240868028.sam	117:21:33:28	921.3	182.8	
1240869828.sam	117:22:03:28	621.3	182.6	
1240870728.sam	117:22:18:28	621.3	182.5	
1240871628.sam	117:22:33:28	921.3	182.5	
1240873428.sam	117:23:03:28	621.3	182.5	
1240874328.sam	117:23:18:28	621.3	182.6	
1240875228.sam	117:23:33:28	921.3	182.6	
1240877028.sam	118:00:03:28	621.3	182.5	
1240877928.sam	118:00:18:28	621.3	182.5	
1240878828.sam	118:00:33:28	921.3	182.6	
1240880628.sam	118:01:03:28	621.3	182.6	
1240881528.sam	118:01:18:28	621.3	182.6	
1240882428.sam	118:01:33:28	921.3	182.6	
1240883796.sam	118:01:56:16	171.3	182.2	
1240884228.sam	118:02:03:28	621.3	182.5	
1240885128.sam	118:02:18:28	921.3	182.5	
1240886028.sam	118:02:33:28	621.3	182.6	
1240887396.sam	118:02:56:16	171.3	182.3	
1240887828.sam	118:03:03:28	921.3	182.4	
1240888728.sam	118:03:18:28	621.3	182.6	
1240889628.sam	118:03:33:28	621.3	182.6	
1240890996.sam	118:03:56:16	171.3	182.2	

continued on next page

file name	start time [UTC]	duration [s]	source level	comments
1240891428.sam	118:04:03:28	621.3	182.5	
1240892328.sam	118:04:18:28	621.3	182.4	
1240893228.sam	118:04:33:28	921.3	182.5	
1240894596.sam	118:04:56:16	171.3	182.3	
1240895028.sam	118:05:03:28	621.3	182.5	
1240895928.sam	118:05:18:28	621.3	182.6	
1240896828.sam	118:05:33:28	921.3	182.6	
1240898196.sam	118:05:56:16	171.3	182.4	
1240898628.sam	118:06:03:28	621.3	182.5	
1240899528.sam	118:06:18:28	621.3	182.5	
1240900428.sam	118:06:33:28	921.0	182.5	
1240901796.sam	118:06:56:16	171.3	182.3	
1240902228.sam	118:07:03:28	621.3	182.5	
1240903128.sam	118:07:18:28	621.0	182.5	
1240904028.sam	118:07:33:28	921.0	182.6	
1240905396.sam	118:07:56:16	171.0	182.3	
1240905828.sam	118:08:03:28	621.0	182.5	
1240906728.sam	118:08:18:28	621.0	182.5	
1240907628.sam	118:08:33:28	921.0	182.5	
1240908996.sam	118:08:56:16	171.0	182.3	
1240909428.sam	118:09:03:28	621.0	182.5	
1240910328.sam	118:09:18:28	621.0	181.9	
1240911228.sam	118:09:33:28	921.0	182.5	
1240912596.sam	118:09:56:16	171.0	182.3	
1240913028.sam	118:10:03:28	621.0	182.4	
1240913928.sam	118:10:18:28	621.0	182.4	
1240914828.sam	118:10:33:28	921.0	182.5	
1240916196.sam	118:10:56:16	171.0	182.3	
1240916628.sam	118:11:03:28	621.0	182.5	
1240917528.sam	118:11:18:28	621.0	182.4	
1240918428.sam	118:11:33:28	921.0	182.4	
1240919796.sam	118:11:56:16	171.0	182.3	
1240920228.sam	118:12:03:28	621.0	182.2	
1240921128.sam	118:12:18:28	621.0	182.4	
1240922028.sam	118:12:33:28	921.0	182.4	
1240923396.sam	118:12:56:16	171.0	182.4	
1240923828.sam	118:13:03:28	621.0	182.5	
1240924728.sam	118:13:18:28	621.0	182.4	

continued on next page

file name	start time [UTC]	duration [s]	source level	comments
1240925628.sam	118:13:33:28	921.0	182.4	
1240926996.sam	118:13:56:16	171.0	182.5	
1240927428.sam	118:14:03:28	621.0	182.4	
1240928328.sam	118:14:18:28	621.0	182.5	
1240929228.sam	118:14:33:28	921.0	182.4	
1240930596.sam	118:14:56:16	171.0	182.4	
1240931028.sam	118:15:03:28	621.0	182.2	
1240931928.sam	118:15:18:28	621.0	182.4	
1240932828.sam	118:15:33:28	921.0	182.4	
1240934196.sam	118:15:56:16	171.0	182.1	
1240934628.sam	118:16:03:28	621.0	182.3	
1240935528.sam	118:16:18:28	621.0	182.3	
1240936428.sam	118:16:33:28	921.0	182.4	
1240937796.sam	118:16:56:16	171.0	182.3	
1240938228.sam	118:17:03:28	621.0	182.4	
1240939128.sam	118:17:18:28	621.0	182.5	
1240940028.sam	118:17:33:28	921.0	182.2	
1240941396.sam	118:17:56:16	171.0	182.2	
1240941828.sam	118:18:03:28	621.0	182.5	
1240942728.sam	118:18:18:28	621.0	182.5	
1240943628.sam	118:18:33:28	921.0	182.5	
1240944996.sam	118:18:56:16	171.0	182.2	
1240945428.sam	118:19:03:28	621.0	182.4	
1240946328.sam	118:19:18:28	621.0	182.5	
1240947228.sam	118:19:33:28	921.0	182.4	
1240948596.sam	118:19:56:16	171.0	182.3	
1240949028.sam	118:20:03:28	621.0	182.4	
1240949928.sam	118:20:18:28	621.0	180.9	
1240950828.sam	118:20:33:28	921.0	182.5	
1240952196.sam	118:20:56:16	171.0	182.4	
1240952628.sam	118:21:03:28	621.0	182.5	
1240953528.sam	118:21:18:28	621.0	182.5	
1240954428.sam	118:21:33:28	921.0	182.7	
1240955796.sam	118:21:56:16	171.0	182.3	
1240956228.sam	118:22:03:28	621.0	182.5	
1240957128.sam	118:22:18:28	621.0	182.6	
1240958028.sam	118:22:33:28	921.0	182.5	
1240959396.sam	118:22:56:16	171.0	182.7	

continued on next page

file name	start time [UTC]	duration [s]	source level	comments
1240959828.sam	118:23:03:28	621.0	182.5	
1240960728.sam	118:23:18:28	621.0	182.4	
1240961628.sam	118:23:33:28	921.0	182.4	
1240962996.sam	118:23:56:16	171.0	182.3	
1240963428.sam	119:00:03:28	621.0	182.4	
1240964328.sam	119:00:18:28	621.0	182.5	
1240965228.sam	119:00:33:28	921.0	182.5	
1240966596.sam	119:00:56:16	171.0	182.4	
1240967028.sam	119:01:03:28	621.0	182.5	
1240967928.sam	119:01:18:28	621.0	181.7	
1240968828.sam	119:01:33:28	921.0	182.4	
1240970628.sam	119:02:03:28	621.0	182.4	
1240971528.sam	119:02:18:28	241.0	181.7	Aborted
1240972428.sam	119:02:33:28	921.0	182.4	
1240973796.sam	119:02:56:16	171.0	182.3	
1240974228.sam	119:03:03:28	621.0	182.5	
1240975128.sam	119:03:18:28	621.0	182.4	
1240976028.sam	119:03:33:28	921.0	182.5	
1240977396.sam	119:03:56:16	171.0	182.2	
1240977828.sam	119:04:03:28	621.0	182.8	
1240978728.sam	119:04:18:28	621.0	182.4	
1240979628.sam	119:04:33:28	921.0	182.4	
1240980996.sam	119:04:56:16	171.0	182.2	
1240981428.sam	119:05:03:28	621.0	182.2	
1240982328.sam	119:05:18:28	621.0	182.2	
1240983228.sam	119:05:33:28	921.0	182.4	
1240984596.sam	119:05:56:16	171.0	182.2	
1240985028.sam	119:06:03:28	621.0	185.7	
1240985928.sam	119:06:18:28	621.0	183.0	
1240986828.sam	119:06:33:28	921.0	187.9	
1240988196.sam	119:06:56:16	171.0	182.4	
1240988628.sam	119:07:03:28	621.0	182.2	
1240989528.sam	119:07:18:28	621.0	182.2	
1240990428.sam	119:07:33:28	921.0	182.4	
1240991796.sam	119:07:56:16	171.0	182.1	
1240992228.sam	119:08:03:28	621.0	182.3	
1240993128.sam	119:08:18:28	621.0	182.4	
1240994028.sam	119:08:33:28	921.0	182.3	

continued on next page

file name	start time [UTC]	duration [s]	source level	comments
1240995396.sam	119:08:56:16	171.0	182.0	
1240995828.sam	119:09:03:28	621.0	182.2	
1240996728.sam	119:09:18:28	621.0	182.2	
1240997628.sam	119:09:33:28	921.0	182.3	
1240998996.sam	119:09:56:16	171.0	182.1	
1240999428.sam	119:10:03:28	621.0	182.3	
1241000328.sam	119:10:18:28	621.0	182.3	
1241001228.sam	119:10:33:28	921.0	182.4	
1241002596.sam	119:10:56:16	171.0	182.2	
1241003028.sam	119:11:03:28	621.0	182.3	
1241003928.sam	119:11:18:28	621.0	182.2	
1241004828.sam	119:11:33:28	921.0	182.2	
1241006196.sam	119:11:56:16	171.0	182.0	
1241006628.sam	119:12:03:28	621.0	182.2	
1241007528.sam	119:12:18:28	621.0	182.2	
1241008428.sam	119:12:33:28	921.0	182.3	
1241009796.sam	119:12:56:16	171.0	182.3	
1241010228.sam	119:13:03:28	621.0	182.2	
1241011128.sam	119:13:18:28	621.0	182.2	
1241012028.sam	119:13:33:28	921.0	182.2	
1241013396.sam	119:13:56:16	171.0	182.1	
1241013828.sam	119:14:03:28	621.0	182.4	
1241014728.sam	119:14:18:28	621.0	182.3	
1241015628.sam	119:14:33:28	921.0	184.3	
1241016996.sam	119:14:56:16	171.0	182.1	
1241017428.sam	119:15:03:28	621.0	182.1	
1241018328.sam	119:15:18:28	621.0	182.3	
1241019228.sam	119:15:33:28	921.0	183.2	
1241020596.sam	119:15:56:16	171.0	182.4	
1241021028.sam	119:16:03:28	87.8	165.4	Aborted

REPORT DOCUMENTATION PAGE

Form Approved
OPM No. 0704-0188

1. AGENCY USE ONLY	2. REPORT DATE	3. REPORT TYPE AND DATES COVERED
	December 2009	Technical Report

4. TITLE AND SUBTITLE

The APL-UW Multiport Acoustic Projector System

5. FUNDING NUMBERS

N00014-03-1-0181,
N00014-07-1-0743,
N00014-08-1-0843

6. AUTHOR(S)

Rex K. Andrew

7. PERFORMING ORGANIZATION NAME(S) AND ADDRESS(ES)

Applied Physics Laboratory
University of Washington
1013 NE 40th Street
Seattle, WA 98105-6698

8. PERFORMING ORGANIZATION REPORT NUMBER

9. SPONSORING / MONITORING AGENCY NAME(S) AND ADDRESS(ES)

Dr. Ellen Livingston
Office of Naval Research, Code 321OA
One Liberty Center
875 North Randolph Street Suite 1425
Arlington, VA 22203-1995

10. SPONSORING / MONITORING AGENCY REPORT NUMBER

11. SUPPLEMENTARY NOTES

12a. DISTRIBUTION / AVAILABILITY STATEMENT

Approved for public release; distribution is unlimited.

12b. DISTRIBUTION CODE

13. ABSTRACT *(Maximum 200 words)*

The Applied Physics Laboratory of the University of Washington (APL-UW) has acquired on loan an experimental device known as the multiport transducer. APL-UW has developed, in turn, a complete transmitter system that integrated this transducer, capable of wideband operation (roughly 180–350 Hz) from near-surface depths to depths greater than 1000 m. The system's electrical components include an autotransformer tuner, a sea battery, and a fibre optic telemetry interface; mechanical components include a steel supporting structure and a pressure-compensated tuner housing; an additional acoustical component is a monitor hydrophone in a vibration isolation mount; and a signal component involves a lumped parameter SPICE circuit model approximation of the entire end-to-end system, an associated C++ application to predict the time-domain acoustic far field from a standard time-domain waveform input file, and a pre-equalization filter. The multiport system was a key element in a 2009 at-sea acoustics experiment located in the Philippine Sea and provided many hours of high-quality pulsed transmissions to a nearby vertical line array of hydrophones.

14. SUBJECT TERMS

Underwater acoustic transducer, Multiport source, Signal equalization, Ocean acoustic tomography, PhilSea09

15. NUMBER OF PAGES

102

16. PRICE CODE

17. SECURITY CLASSIFICATION OF REPORT	18. SECURITY CLASSIFICATION OF THIS PAGE	19. SECURITY CLASSIFICATION OF ABSTRACT	20. LIMITATION OF ABSTRACT
Unclassified	Unclassified	Unclassified	SAR